Copy 6
RM L52K25

NACA RM L52K25

RESEARCH MEMORANDUM

INVESTIGATION OF THE EFFECT OF CHORDWISE POSITIONING AND SHAPE OF AN UNDERWING NACELLE ON THE HIGH-SPEED AERODYNAMIC CHARACTERISTICS OF A 45° SWEPTBACK TAPERED-IN-THICKNESS-RATIO WING OF ASPECT RATIO 6

By H. Norman Silvers and Thomas J. King, Jr.

Langley Aeronautical Laboratory
Langley Field, Va.

NATIONAL ADVISORY COMMITTEE
FOR AERONAUTICS

WASHINGTON
January 22, 1953

NATIONAL ADVISORY COMMITTEE FOR AERONAUTICS

RESEARCH MEMORANDUM

INVESTIGATION OF THE EFFECT OF CHORDWISE POSITIONING AND SHAPE OF AN UNDERWING NACELLE ON THE HIGH-SPEED AERODYNAMIC CHARACTERISTICS OF A 45° SWEPTBACK TAPERED-IN-THICKNESS-RATIO WING OF ASPECT RATIO 6

By H. Norman Silvers and Thomas J. King, Jr.

SUMMARY

Three different nacelles located in an underwing position at the 0.46 semispan station of a 45° sweptback wing were investigated at three chordwise positions through a Mach number range from 0.70 to 1.08. The nacelle profiles were essentially an ogive cylinder, an NACA 65A-series airfoil, and an NACA 0-series airfoil (reversed). The model was a small-scale semispan wing of aspect ratio 6 and tapered-in-thickness ratio.

The results showed that, at Mach numbers greater than 0.95, the lowest nacelle-drag coefficients were obtained with the NACA 65A-series shape in rearward and intermediate chordwise positions and with the ogive-cylinder shape in the forward position. Of the chordwise positions investigated, the rearward nacelle position generally gave the lowest nacelle-drag coefficients and the highest drag-divergence Mach numbers. Of the aerodynamic characteristics other than those involving drag, the stability characteristics showed the largest effects of adding a nacelle to the model. At a Mach number of 1.08, where the largest changes in stability at a lift coefficient of 0.1 usually occurred, a forward nacelle position was destabilizing by an amount equivalent to a change in aerodynamic-center location of as much as 15 percent of the mean aerodynamic chord. The destabilizing effect of forward nacelles was reduced by rearward movement of the nacelles. The stability characteristics at the higher lift coefficients showed that both the ogive-cylinder shape and the 65A-series shape in forward and intermediate chordwise positions extended the lift coefficient at which pitch-up was shown for the wing without nacelles. The 0-series shape extended the lift coefficient for pitch-up for all chordwise locations of the nacelle.

INTRODUCTION

The National Advisory Committee for Aeronautics is conducting a program of research on nacelles and external stores in order to provide installations suitable for use on airplanes at transonic speeds. The investigations of this program are concerned with an over-all evaluation of the effects of body positioning and shape on the aerodynamic characteristics of airplane models with straight and sweptback wings.

The present paper is the second of a series of papers reporting the results of investigations made on solid bodies of revolution in the Langley high-speed 7- by 10-foot tunnel as part of the general program. In this paper are presented results showing the effect of chordwise positioning of underwing nacelles of three profile shapes at a wing spanwise location of 0.46 semispan outboard of the plane of symmetry on a 45° sweptback wing without a fuselage. Previously reported (ref. 1) are results showing the effect of spanwise and chordwise positioning of an underwing, ogive-cylinder nacelle on a 45° sweptback wing without a fuselage.

In the investigations of nacelles made in the 7- by 10-foot tunnel as well as those made earlier by the Pilotless Aircraft Research Division (refs. 2 to 6) a wing of 45° sweepback, aspect ratio 6, taper ratio 0.6, and NACA 65A-series airfoil sections has been used as the test vehicle. The thickness of the wing used in the tunnel investigations tapered from 9 percent chord at the root to 3 percent chord at the tip, while the thickness of the wing of the flight models was 9-percent chord from root to tip. For the most part, the investigations were made on solid nacelle models. The effects of internal flow are, however, shown for one nacelle location in reference 6, and for several nacelle locations in another investigation (ref. 7) made in the Langley 8-foot high-speed tunnel.

The results obtained in the investigations of which this paper is one are considered to be exploratory in nature. By covering a broad range of nacelle positioning variables, these results are intended to show positions of particular interest in order that later investigations may be directed toward developing a better understanding of the flow characteristics over these installations. These papers are also intended to supplement the zero-lift drag results obtained in earlier flight investigations (refs. 2 to 6) by covering a range of lift coefficients extending from about 0 to about 0.5 and also by showing the effects of nacelle geometry and positioning on wing lift, pitching moment, and bending moment.

SYMBOLS

C_L	lift coefficient (Twice semispan lift/qS_w)
C_D	drag coefficient (Twice semispan drag/qS_w)
C_{D_n}	nacelle-drag coefficient $\left(C_{D_{\text{model + nacelle}}} - C_{D_{\text{model}}}\right) \frac{S_w}{2S_n}$
C_m	pitching-moment coefficient referred to 0.25$\bar{c}$ of wing (Twice semispan pitching moment/$qS_w\bar{c}$)
C_B	bending-moment coefficient $\left(\text{Twice root bending moment}/qS_w\frac{b}{2}\right)$
q	free-stream dynamic pressure, lb/sq ft, $\frac{1}{2}\rho V^2$
S_w	twice area of semispan model, 0.125 sq ft
S_n	maximum frontal area of nacelle, 0.00119 sq ft
$\bar{c}$	mean aerodynamic chord of wing, 0.147 ft $\left[\frac{2}{S_w}\int_0^{b/2} c^2 dy \text{ (using theoretical tip)}\right]$
c	local wing chord parallel to chord plane, ft
b	twice span of semispan model, 0.866 ft
d	nacelle diameter, ft
d_i	diameter of nacelle at hypothetical nacelle inlet, ft
d_e	diameter of nacelle at hypothetical nacelle exit, ft
x	longitudinal distance from wing leading edge to nose of nacelle; negative when nose of nacelle is forward of wing leading edge, ft
y	lateral distance from plane of symmetry to center line of nacelle, ft
l,	nacelle length, ft
V	effective free-stream air velocity, ft/sec

M effective free-stream Mach number $\left[\frac{2}{S_w}\int_0^{b/2} cM_a dy\right]$

M_l local Mach number

M_a average chordwise Mach number

ρ mass density of air, slugs/cu ft

α angle of attack, deg

y_{cp} lateral center of pressure referred to wing semispan, $\frac{\partial C_B}{\partial C_L}$

$C_{L_\alpha} = \left(\frac{\partial C_L}{\partial \alpha}\right)_M$

$C_{m_{C_L}} = \left(\frac{\partial C_m}{\partial C_L}\right)_M$

APPARATUS AND MODELS

This investigation utilized a small semispan model that was mounted on a reflection-plane plate, located 3 inches from the tunnel wall in order to bypass the wall boundary layer (fig. 1). A more detailed discussion of the model setup and the strain-gage-balance system employed is given in reference 1.

The wing was constructed of steel and had 45° of sweepback referred to the quarter-chord line, an aspect ratio of 6, and a taper ratio of 0.6. The airfoil section at the wing root was an NACA 65A009 and at the wing tip an NACA 65A003 section.

The nacelles were solid bodies of revolution constructed of mahogany. Three nacelle shapes were investigated. They were an ogive-cylinder shape, a shape generated by revolving an NACA 65A-series airfoil section, and a shape generated by revolving a modified NACA 0-series airfoil section which was reversed in direction for this investigation. A drawing of the nacelles with the nacelle ordinates is presented in figure 2. The nacelles were designed to have identical maximum diameters and, if ducted, to have approximately equal nacelle diameters at the hypothetical nacelle inlets and exits, as well as identical fineness ratios of the ducted lengths. In order to maintain fineness ratios that were approximately the same for the unducted nacelles, it was necessary to modify both the nose and the tail portions of the NACA 0-series profile. The fineness

ratios of the test nacelles were 9.34 for the ogive-cylinder shape, 10.68 for the 65A-series shape, and 10.04 for the 0-series shape.

The ogive-cylinder nacelle was similar in shape to the nacelle investigated in references 2 to 6, in that for both nacelles ogival-nose and tail sections were used between which was located a cylindrical length of body. For the nacelle of the present investigation, the ogival tail section terminated in a point, whereas the nacelles of references 2 to 6 were blunt-ended; that is, a portion of the ogival tail was removed.

The nacelles used herein were also somewhat larger relative to the wing than were the nacelles of the flight investigations. The size of the nacelles of this investigation was determined from existing jet-engine specifications and by considering the wing to be a 0.01-scale model of a bomber wing. At full scale the diameter of the nacelles would be about 47 inches and the airplane would be of the medium-bomber category of airplanes.

Each of the nacelles was so located below the wing as to maintain a distance equal to the maximum radius of the nacelle between the wing chord plane and the nacelle center line. The nacelles were located at $0.46b/2$ outboard of the wing root chord. Three chordwise positions of the nacelle were investigated and designated herein as rearward, intermediate, and forward. Test locations in terms of wing local chord length are tabulated on figure 3. The chordwise positions of the nacelles were obtained by locating the solid bodies in chordwise positions so that, if the nacelles were ducted, the inlets would be at the wing leading edge for the rearward nacelle; the midlength of the ducted bodies would be at the midchord point for the intermediate nacelle; or the exits of the ducted bodies would be at the wing trailing edge for the forward nacelle. Because of the differing lengths of nacelle ahead of the contemplated inlets, the chordwise position parameter x/c assumes different values for each of the three nacelle shapes at a given chordwise position. No fairing of the wing-nacelle junctures has been employed for any of the configurations used in this investigation.

METHODS AND TESTS

The reflection-plane plate attached to the wall of the high-speed 7- by 10-foot tunnel induces over its surface a region of local velocities higher than the free-stream velocities of the tunnel, which permits testing of small models to Mach numbers of 1.08. The variations in local Mach number over the reflection-plane plate are shown in figure 4 for typical Mach numbers. As indicated by these data the Mach number gradient in the region of the model decreases with decreasing tunnel speed.

At a Mach number of about 0.93 the flow is gradient free. Effective free-stream Mach numbers, which are used as the basis of data presentation, were obtained from the relationship

$$M = \frac{2}{S}\int_0^{b/2} cM_a dy$$

Lift, drag, pitching-moment, and bending-moment coefficients were measured over an angle-of-attack range that extended from about -1.5° to 9.0° at Mach numbers from 0.70 to 1.08. The variation of Reynolds number, based on the mean aerodynamic chord, with Mach number for these tests is shown in figure 5. Because of the small size of the model employed in this investigation, jet-boundary and blockage corrections were considered negligible.

In general, the accuracy of the force and moment measurements can be judged by any random scatter of the test points of the basic data. In determining increments of forces and moments, however, faired values of forces and moments are used; thus, the influence of test-point scatter on the curves of summary results tended to be minimized.

The reflection-plane technique, in which small half-span models are located in a localized high-velocity field to obtain transonic speeds, has sometimes given absolute values of coefficients, particularly drag, that do not correlate well with data obtained on larger full-span models. Valid incremental effects, such as those due to model configuration, lift coefficient, or Mach number are, however, believed to be obtained by this technique. These conclusions were reached after a correlative study of results from bump-type test techniques and the conventional sting-type test techniques had been made (ref. 8.) Subsequent experience with nacelle and external-store-tests, results which are as yet unpublished, has shown that trends of drag increments due to nacelle configuration and obtained from models investigated on bump-type facilities show good qualitative agreement with those obtained on larger-scale full-span models tested in flight.

RESULTS AND DISCUSSION

The results of this investigation are presented in figures, the contents of which are summarized on the following page:

Lift-curve slopes presented were measured through zero lift, whereas pitching-moment-curve slopes were measured at a lift coefficient of 0.1.

DRAG CHARACTERISTICS

The variations in drag coefficient of the model with each of the three nacelles and without the nacelles are presented in figure 10. The data presented in this paper for the nacelle with the ogive-cylinder shape were taken from reference 1.

The Mach number for drag divergence used in this paper was determined by inspection of the drag-coefficient curves (fig. 10) and the discussion is limited to the results at lift coefficients of 0.4 and less. The results indicate that nacelle shape has in general less effect on the drag-divergence Mach number of nacelles in the rearward and forward positions than on the nacelles in the intermediate position. In the intermediate position, nacelle shape shows an increasing importance with increasing lift coefficient. Of the three shapes investigated in an intermediate position, the highest drag-divergence Mach numbers were obtained with the 65A-series shape and the lowest with the ogive-cylinder shape. Furthermore, it appears that, of the nacelle chordwise positions investigated, the higher drag-divergence Mach numbers were generally obtained, up to $C_L = 0.4$, with nacelles in the rearward position.

The variation of the nacelle-drag coefficients, which are defined as the increments in drag due to the nacelles based upon the nacelle maximum frontal area and include interference, are presented in figure 11 as a function of Mach number. These data have been used to cross-plot the nacelle-drag coefficient against both model lift coefficient (fig. 12) and nacelle chordwise position (fig. 13).

In reference 1, it was shown that the largest effect of increase in model lift coefficient on nacelle-drag coefficient was obtained for the extreme inboard and tip location of the nacelle, and conversely nacelle-drag coefficients for midspan locations were less affected by increase in model lift than extreme spanwise locations. The results presented herein (fig. 12) also indicate that at the midspan location investigated,

increase in lift had little over-all effect on the nacelle-drag coefficients, except for some rather abrupt increases in C_{D_n} at lift coefficients of about 0.3 and greater which occurred for the most part at subsonic Mach numbers with rearward locations of the previously investigated ogive-cylinder shape and also for the 65A-series shape.

At Mach numbers greater than about 0.95 at the lower lift coefficients and at all Mach numbers at the higher lift coefficients, both nacelle chordwise location and shape have important effects on the nacelle-drag coefficients. These effects are illustrated in figure 13 for Mach numbers of 0.7, 0.9, and 1.08. At Mach numbers lower than 0.95 at the lower lift coefficients, the nacelle-drag coefficients are considerably smaller and less affected by nacelle position and shape. Rearward nacelle movement is seen to result in substantial reductions in nacelle-drag coefficients at a Mach number of 1.08 at all lift coefficients and as a result the minimum nacelle drag is obtained with the most rearward nacelle. Of the nacelle shapes investigated the lowest nacelle-drag coefficients are shown (figs. 11 to 13) for the 65A-series shape in rearward and intermediate chordwise positions at Mach numbers greater than about 0.95 and at lift coefficients from 0 to 0.4. In the forward position the lowest nacelle drag for supersonic Mach numbers and lift coefficients from 0 to 0.4 is shown for the 0-series shape. At a lift coefficient of 0.5 and at subsonic speeds, the chordwise location for minimum nacelle drag in general has changed from the most rearward location investigated to more forward locations. It appears (fig. 12) that this change takes place at lift coefficients of about 0.3 or greater.

It has been expected that nacelle shapes having a cylindrical midsection might produce smaller nacelle-drag coefficients than nacelle shapes with continuously varying curvatures of less severe effects of superposition of the pressures over the cylindrical length of the body on the pressure field of the wing. The results presented herein, however, show an obvious drag disadvantage for a nacelle of such a shape. This result may be due to the fact that the length of cylinder employed is less than the length of the local wing chord. Thus, the regions of peak pressures at the intersections of the nose and the tail sections with the cylindrical midsection, although not necessarily coinciding with the peak pressures of the wing, still lie on some part of the wing for all nacelle chordwise positions investigated. The resulting interference appears to be more serious for the ogive-cylinder than for the two shapes with continuously varying curvature. It would appear necessary to design bodies of the ogive-cylinder shape with a cylindrical midsection long enough to locate the peak pressures ahead of and behind the local wing chord. Such a design specification would seem to introduce some specific limits as to what may be efficiently housed in a body with an ogive-cylinder shape.

It should be remembered that the results presented in this paper were obtained on a wing without a fuselage. As suggested in reference 1,

it appears that a fuselage can have an appreciable effect on nacelle interference and consequently on nacelle drag at transonic speeds. It further appears that the effects of a fuselage on C_{D_n} can be larger for extreme inboard as well as extreme tip locations of a nacelle than for intermediate locations. Hence, it might be anticipated that the nacelle-drag results presented herein for an intermediate spanwise nacelle location would be less affected by a fuselage than those obtained for either more inboard or more outboard nacelle locations.

Lift-Drag Ratios

In figure 14 are presented the maximum lift-drag ratios obtained for the model with and without nacelles. In evaluating the effect of nacelles on $(L/D)_{max}$ it has been found convenient to divide the maximum lift-drag ratio of the model with nacelle by the maximum lift-drag ratio of the model without nacelle. The resulting ratio gives a quantitative expression of the effect of the nacelles on $(L/D)_{max}$. These ratios are presented in figure 15 as a function of nacelle chordwise location for representative Mach numbers. The results reflect the characteristics of the nacelle-drag coefficients discussed in the preceding section; that is, the nacelle shapes and positions giving the lowest drag due to the nacelle also give the highest maximum lift-drag ratios. It is seen that at a Mach number of 1.08 where the most significant effects of nacelle shape and position were shown in the drag characteristics, the highest $(L/D)_{max}$ was obtained with the 65A-series shape, and for all shapes the highest $(L/D)_{max}$ was obtained with the rearward nacelle. In the rearward position the maximum lift-drag ratio of the model with the 65A-series nacelle was about 95 percent of the maximum lift-drag ratio of the model without nacelles at $M = 1.08$ and about 97 percent at $M = 0.90$. Throughout the greater part of the Mach number range and the chordwise-position range, the lowest maximum lift-drag ratios were obtained with the nacelle of ogive-cylinder shape, which also gave higher nacelle-drag coefficients than either the 0-series or the 65A-series shapes. At a Mach number of 1.08 the maximum lift-drag ratio of the 65A-series shape was from 6 to 12 percent higher (based on the maximum lift-drag ratio of the basic model) than that of the ogive-cylinder shape throughout the range of chordwise positions investigated.

Lift Characteristics

The variations in lift-curve slope of the model with and without nacelles are presented in figure 16. The increments between the results obtained on the model with and without nacelles are presented in figure 17 as a function of nacelle chordwise position. The increments were obtained

by subtracting the results obtained on the model without the nacelle from those obtained on the model with the nacelle. The largest effect of nacelle shape as well as chordwise position appears at the lower subsonic Mach numbers (represented in fig. 16 by results at $M = 0.70$) where all shapes produce a substantial increase in C_{L_α} of the model for intermediate nacelle chordwise positions with the largest increases being produced by 65A-series shape. At Mach numbers around 0.90 the ogive-cylinder nacelle in the intermediate position is seen to develop a large increase in C_{L_α} (fig. 16). The nacelles of all three shapes in forward positions generally result in little change in C_{L_α} of the model throughout the speed range. At a supersonic Mach number of 1.08 a rearward location of the nacelles results in an increased lift-curve slope of the model that is somewhat less, however, than the increase in C_{L_α} produced by intermediate nacelles at subsonic speeds.

Pitch Characteristics

The slopes of the pitching-moment curves obtained at a lift coefficient of 0.1 for the model with and without nacelles are presented in figure 18. The increments in slope due to the nacelle as a function of nacelle chordwise position obtained from these results are presented in figure 19. The increments were obtained by subtracting the results obtained on the model without the nacelle from those obtained on the model with the nacelle. These data indicate that, at a C_L of 0.1, addition of the nacelles in the forward position is destabilizing by amounts equivalent to changes in the aerodynamic-center location of up to 15 percent of the mean aerodynamic chord. In general, rearward movement of the nacelles results in a substantial stabilizing effect. The effects of nacelle chordwise location are particularly large at $M = 1.08$ where a change in $\Delta C_{m_{C_L}}$ equivalent to a stabilizing change in the aerodynamic-center location of 17 percent of the mean aerodynamic chord occurs for a change from forward to rearward location for the nacelle with the 65A-series shape. Similar changes in $\Delta C_{m_{C_L}}$ were obtained with the 0-series and the ogive-cylinder shapes at this Mach number. The effect of nacelle shape on the stability characteristics of the model is seen (fig. 18) to depend upon Mach number. At the lower subsonic Mach numbers change in nacelle shape from either the 65A-series or the 0-series to the ogive-cylinder shape is stabilizing except for forward positions where nacelle shape has little effect on the stability characteristics. At supersonic Mach numbers the largest effects of the nacelles on the stability characteristics of the model exist for the forward chordwise position and, as indicated above, the maximum change in $C_{m_{C_L}}$ due to the addition of the nacelle is of the order of 0.15.

It is seen in figure 6 that a destabilizing break develops at the higher lift coefficients in the pitching-moment curves of the model without

nacelles at Mach numbers from 0.70 to 1.05. Inspection of the pitching-moment curves of the model with nacelles indicates that some chordwise positions of the nacelles are effective in increasing the lift coefficient at which this pitch-up tendency of the wing develops. In this respect, forward and intermediate locations of both the ogive-cylinder shape and the 65A-series shape are beneficial except at a Mach number of 1.00 (figs. 7 and 8). The 0-series shape, however, appears to increase the lift coefficient for pitch up for all chordwise locations and Mach numbers except at $M = 1.00$ for forward and rearward positions and $M = 1.00$ and 1.05 for the intermediate position.

Lateral Center of Pressure

The incremental effect of the nacelles on the lateral center-of-pressure locations of the model are presented in figure 21 as a function of nacelle chordwise position. These increments were obtained from figure 20 by subtracting the results obtained on the model without the nacelle from those on the model with the nacelle. At the lowest Mach number investigated the nacelles in any chordwise position result in a location of the lateral center of pressure inboard of that for the model without nacelles. Increase in Mach number results in a general outboard movement of y_{cp} due to the nacelles. The largest effect of speed and chordwise position on the location of the lateral center of pressure is shown for the ogive-cylinder shape in an intermediate chordwise position, where about a 3.5-percent semispan outboard change in y_{cp} takes place over a Mach number range from 0.70 to 1.08. As a result of this change in y_{cp} for an intermediate chordwise position, the ogive-cylinder shape experiences a considerable change with speed in the shape of the curve of Δy_{cp} as a function of nacelle chordwise position. The curve is characterized at $M = 0.70$ by the most inboard location of y_{cp} occurring for the intermediate position which changes to the most outboard location of y_{cp} at $M = 1.08$.

CONCLUSIONS

An investigation of the effect of nacelle chordwise positioning and shape of an underwing nacelle on the high-speed aerodynamic characteristics of a small-size 45° sweptback tapered-in-thickness-ratio wing of aspect ratio 6 indicate the following conclusions:

1. The largest effects of nacelle chordwise positioning and shape on the drag characteristics were found at Mach numbers greater than about 0.95.

2. At Mach numbers greater than 0.95 the lowest nacelle-drag coefficients were obtained with the 65A-series shape in the rearward and the intermediate chordwise positions and with the 0-series shape in the forward position.

3. Of the chordwise positions investigated the lowest nacelle-drag coefficients were obtained at the higher Mach numbers and lower lift coefficients with the nacelles in the rearward position.

4. The largest effect of nacelle shape on drag-divergence Mach number was shown for an intermediate chordwise nacelle position where the highest drag divergence Mach numbers were obtained with the 65A-series shape. It also appeared that, in general for any shape, somewhat higher drag-divergence Mach numbers were obtained with a rearward chordwise position of the nacelle than with either intermediate or forward positions.

5. At the higher Mach numbers the highest maximum lift-drag ratios of the model with the nacelles were obtained with the 65A-series shape in the rearward position and in general the lowest were obtained with all chordwise positions of the ogive-cylinder shape.

6. Aside from effects on those characteristics involving drag, perhaps the most important effects of adding a nacelle to the model were shown in the locations of the aerodynamic center. At a Mach number of 1.08 where the largest changes in stability at a lift coefficient of 0.1 usually occurred, a forward position of the nacelle shapes was destabilizing by an amount equivalent to a change in aerodynamic-center location of as much as 15 percent of the mean aerodynamic chord. The destabilizing effect of forward nacelles was reduced by rearward movement of the nacelles.

7. The stability characteristics at the higher lift coefficients showed that forward and intermediate locations of both the ogive-cylinder shape and the 65A-series shape were effective in increasing the lift coefficient at which pitch-up was shown for the wing without nacelles. The 0-series shape was, however, effective in all chordwise locations in increasing the lift coefficient for model pitch-up.

Langley Aeronautical Laboratory,
National Advisory Committee for Aeronautics,
Langley Field, Va.

REFERENCES

1. Silvers, H. Norman, and King, Thomas J., Jr.: A Small-Scale Investigation of the Effect of Spanwise and Chordwise Positioning of an Ogive-Cylinder Underwing Nacelle on the High-Speed Aerodynamic Characteristics of a 45° Sweptback Tapered-in-Thickness Wing of Aspect Ratio 6. NACA RM L52J22, 1952.

2. Pepper, William B., Jr., and Hoffman, Sherwood: Transonic Flight Tests To compare the Zero-Lift Drag of Underslung and Symmetrical Nacelles Varied Chordwise at 40 Percent Semispan of a 45° Sweptback, Tapered Wing. NACA RM L50G17a, 1950.

3. Pepper, William B., Jr., and Hoffman, Sherwood: Comparison of the Zero-Lift Drags Determined by Flight Tests at Transonic Speeds of Symmetrically Mounted Nacelles in Various Spanwise Positions on a 45° Sweptback Wing and Body Combination. NACA RM L51D06, 1951.

4. Hoffman, Sherwood: Comparison of Zero-Lift Drag Determined by Flight Tests at Transonic Speeds of Pylon, Underslung, and Symmetrically Mounted Nacelles at 40 Percent Semispan of a 45° Sweptback Wing and Body Combination. NACA RM L51D26, 1951.

5. Hoffman, Sherwood: Transonic Flight Tests To Compare the Zero-Lift Drags of Underslung Nacelles Varied Spanwise on a 45° Sweptback Wing and Body Combination. NACA RM L52D04a, 1952.

6. Hoffman, Sherwood, and Pepper, William B., Jr.: Transonic Flight Tests To Determine Zero-Lift Drag and Pressure Recovery of Nacelles Located at the Wing Tips on a 45° Sweptback Wing and Body Combination. NACA RM L51K02, 1952.

7. Bielat, Ralph P., and Harrison, Daniel E.: A Transonic Wind-Tunnel Investigation of the Effects of Nacelle Shape and Position on the Aerodynamic Characteristics of Two 47° Sweptback Wing-Body Configurations. NACA RM L52G02, 1952.

8. Donlan, Charles J., Myers, Boyd C., II, and Mattson, Axel T.: A Comparison of the Aerodynamic Characteristics at Transonic Speeds of Four Wing-Fuselage Configurations as Determined From Different Test Techniques. NACA RM L50H02, 1950.

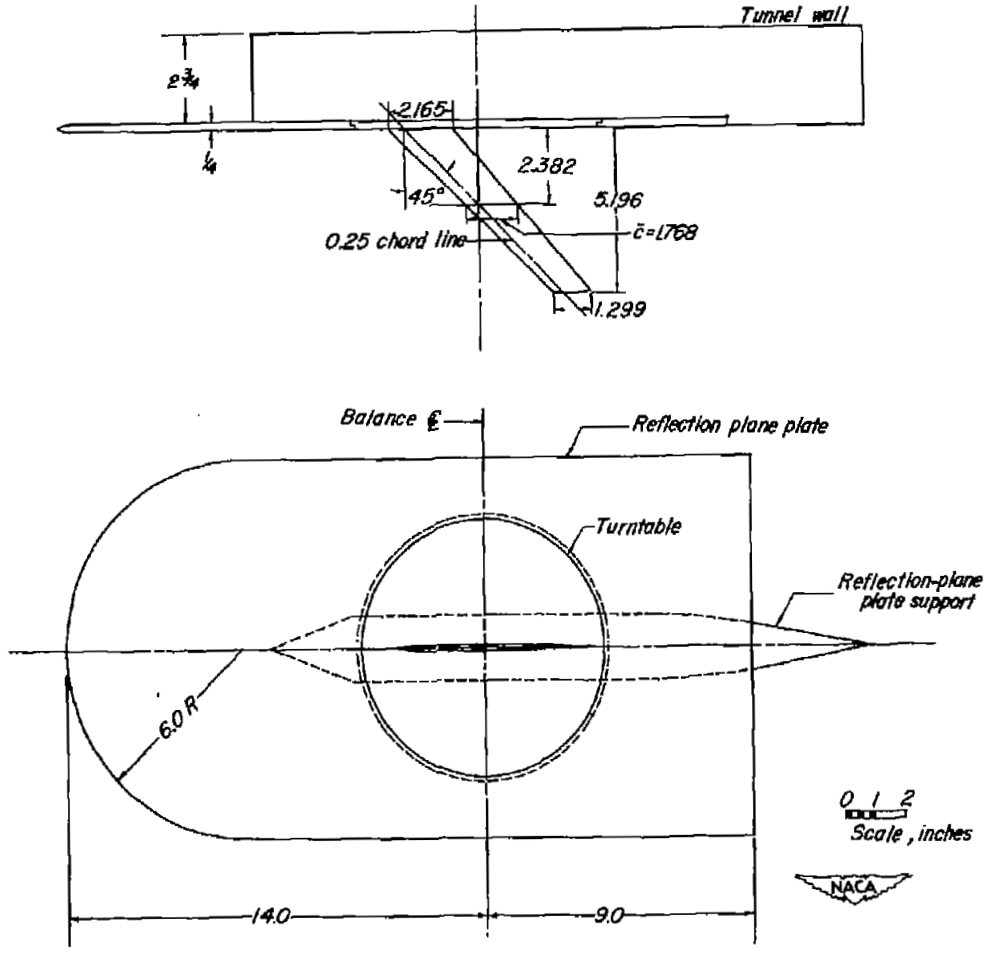

Figure 1.- Two-view drawing of the test setup and the 45° sweptback semispan wing of aspect ratio 6, taper ratio 0.6, and an NACA 65A-series airfoil section tapered in thickness from 9 percent at the root to 3 percent at the tip.

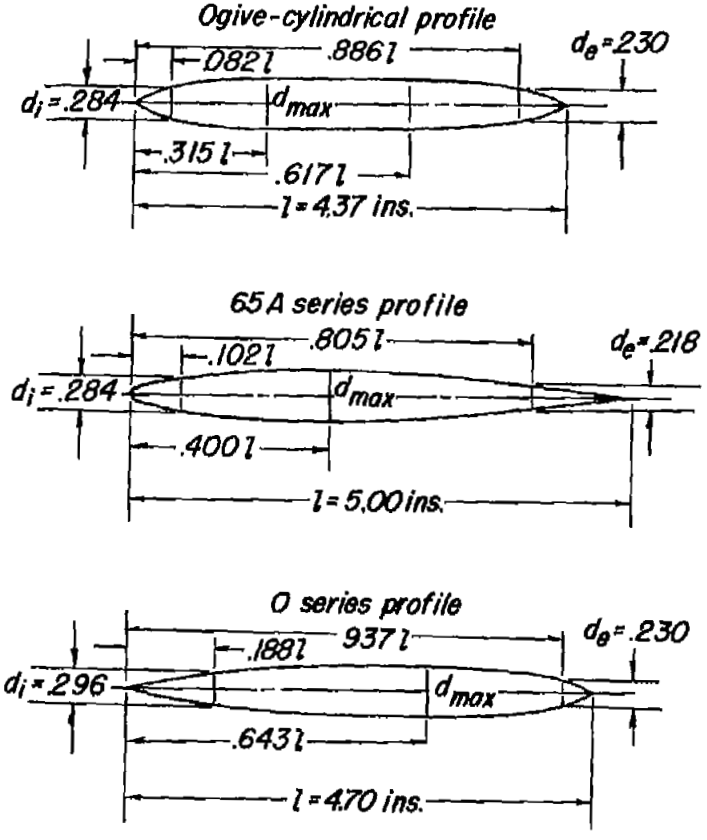

Ogive-cylindrical profile

Fineness ratio 9.34	
Ordinates, percent length	
Station	Radius
0	0
.36	.30
1.21	.73
3.06	1.44
4.87	2.09
6.71	2.65
8.26	3.07
9.15	3.29
9.69	3.44
10.84	3.70
11.99	3.94
13.14	4.12
14.29	4.30
15.44	4.44
17.74	4.70
20.04	4.92
22.34	5.08
24.64	5.20
26.94	5.30
29.24	5.34
31.54	5.36
61.70	5.36
68.59	5.20
74.95	4.76
81.22	3.94
87.48	2.76
90.60	2.11
93.75	1.42
96.89	.72
98.44	.36
100.00	0

65A series profile

Fineness ratio 10.68	
Ordinates, percent length	
Station	Radius
0	0
.50	.72
.75	.87
1.25	1.02
2.50	1.52
5.00	2.04
7.50	2.48
10.00	2.85
15.00	3.43
20.00	3.87
25.00	4.20
30.00	4.44
35.00	4.60
40.00	4.68
45.00	4.67
50.00	4.56
55.00	4.34
60.00	4.03
65.00	3.65
70.00	3.22
75.00	2.73
80.00	2.20
85.00	1.66
90.00	1.11
95.00	.57
100.00	.32
LER = 0.598	

0 series profile

Fineness ratio 10.04	
Ordinates, percent length	
Station	Radius
0	0
5.53	1.30
9.36	2.10
20.20	3.30
27.00	3.77
42.30	4.39
53.40	4.81
64.30	4.96
69.80	4.92
75.40	4.75
80.60	4.45
86.20	3.98
89.00	3.48
91.70	2.94
94.50	2.16
96.30	1.70
97.30	1.28
100.00	0

NACA

Figure 2.- The nacelle profiles.

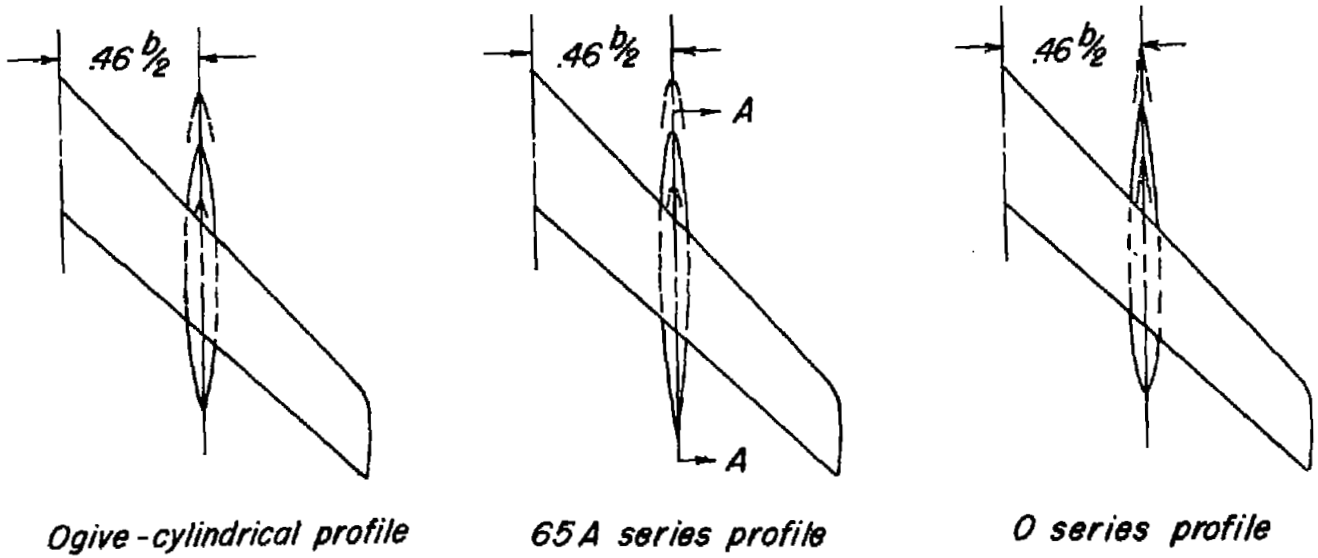

Chord designation	Nacelle Chordwise Location, x/c		
	Ogive-cyl. profile	65A series profile	0 series profile
Forward	-1.192	-1.276	-1.488
Intermediate	-.698	-.784	-.995
Rearward	-.204	-.288	-.500

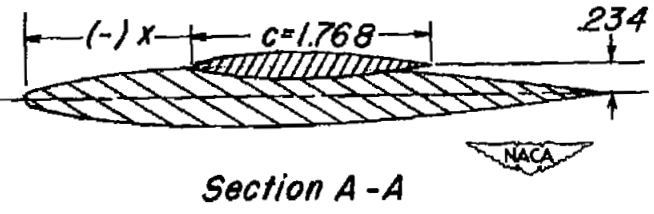

Figure 3.- Locations of the nacelles tested.

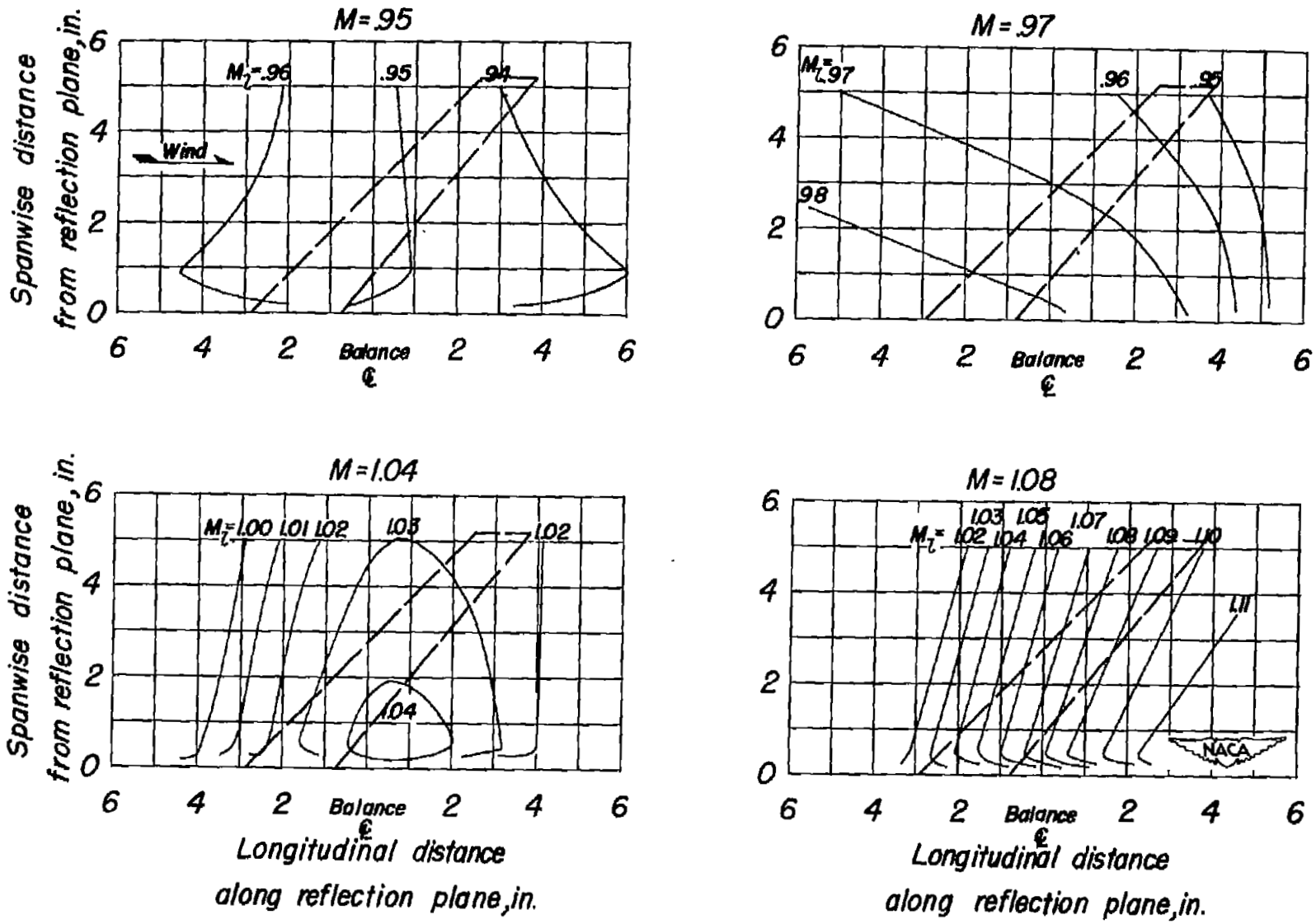

Figure 4.- Typical Mach number contours over side-wall reflection plane in region of model location.

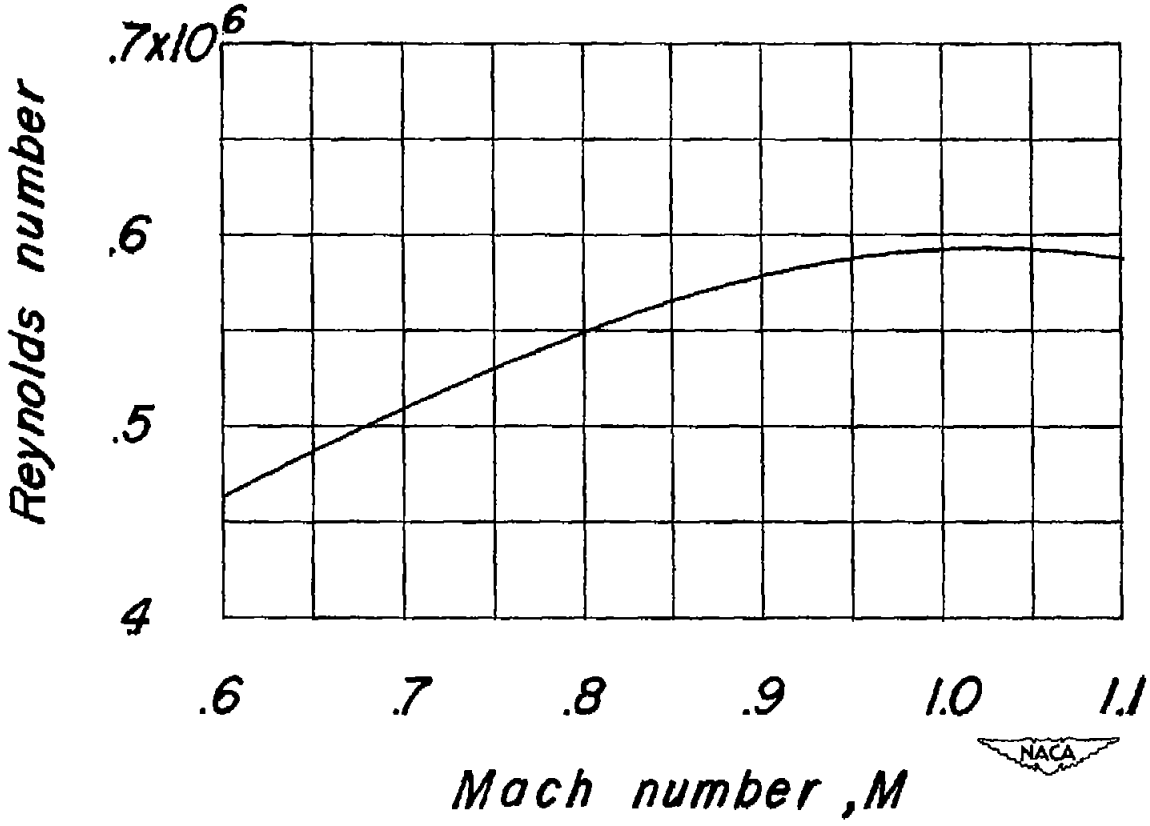

Figure 5.- Variation of Reynolds number with Mach number for the model in the Langley high-speed 7- by 10-foot tunnel.

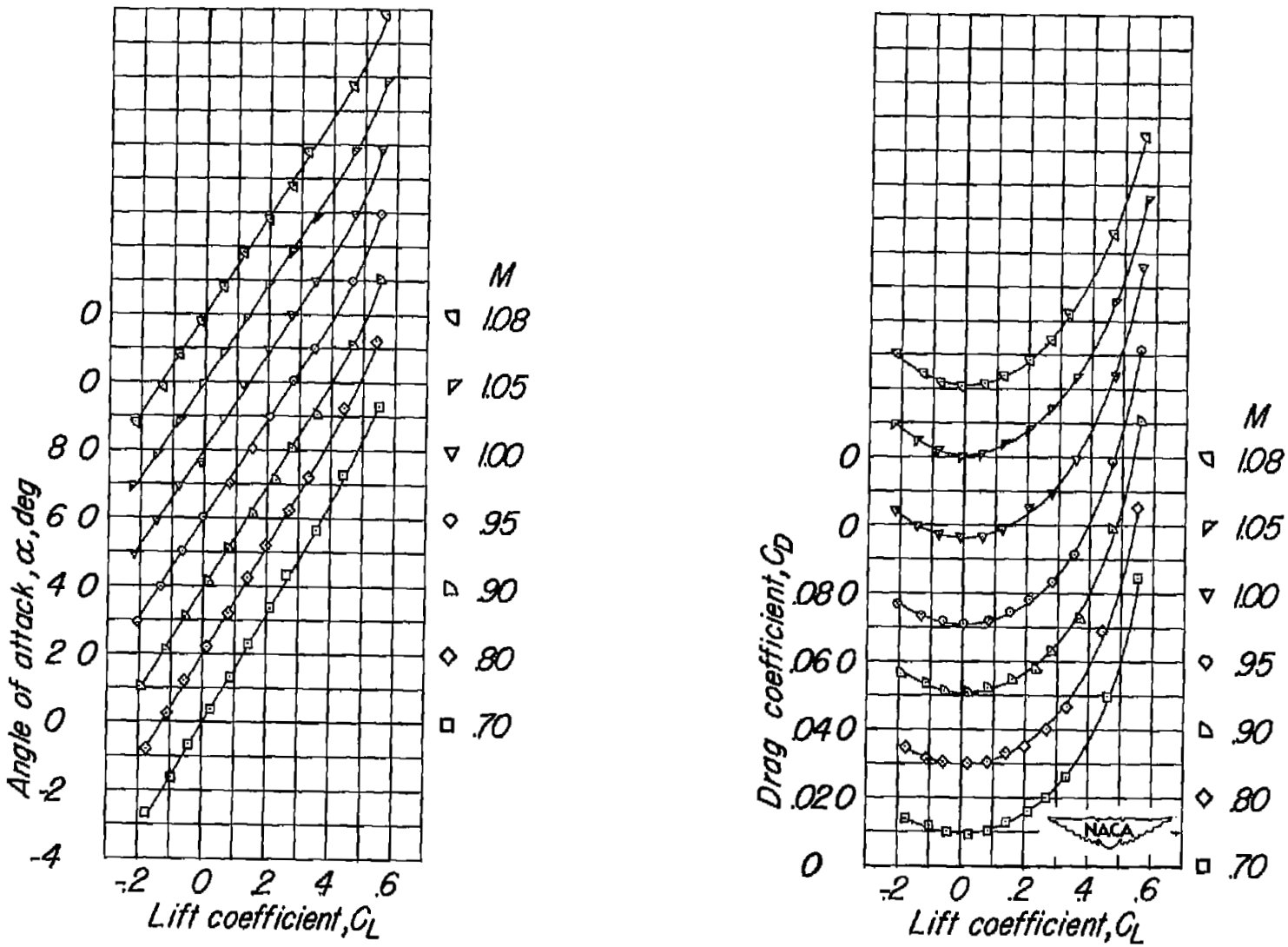

Figure 6.- Aerodynamic characteristics of semispan wing.

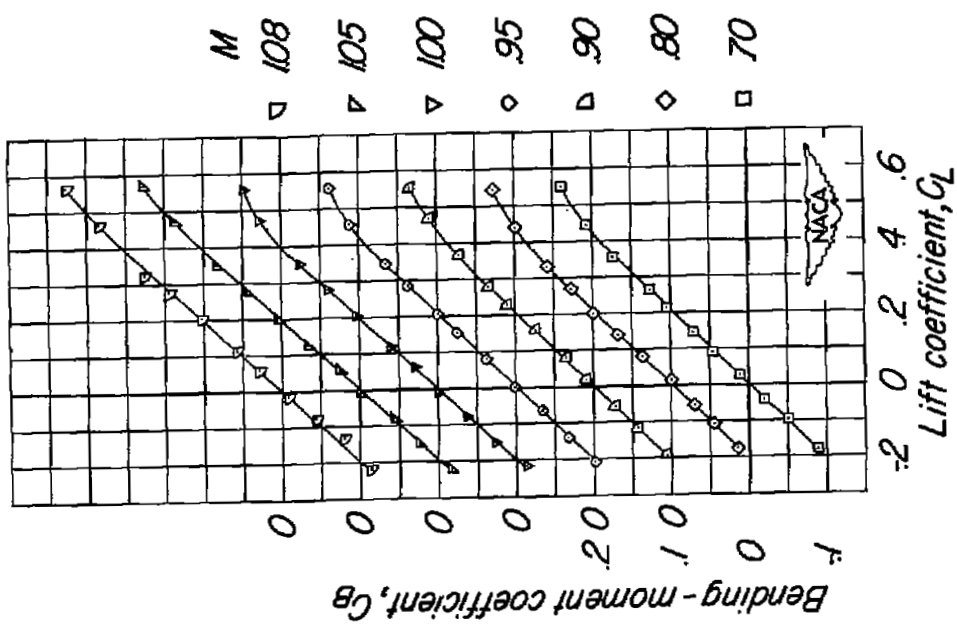

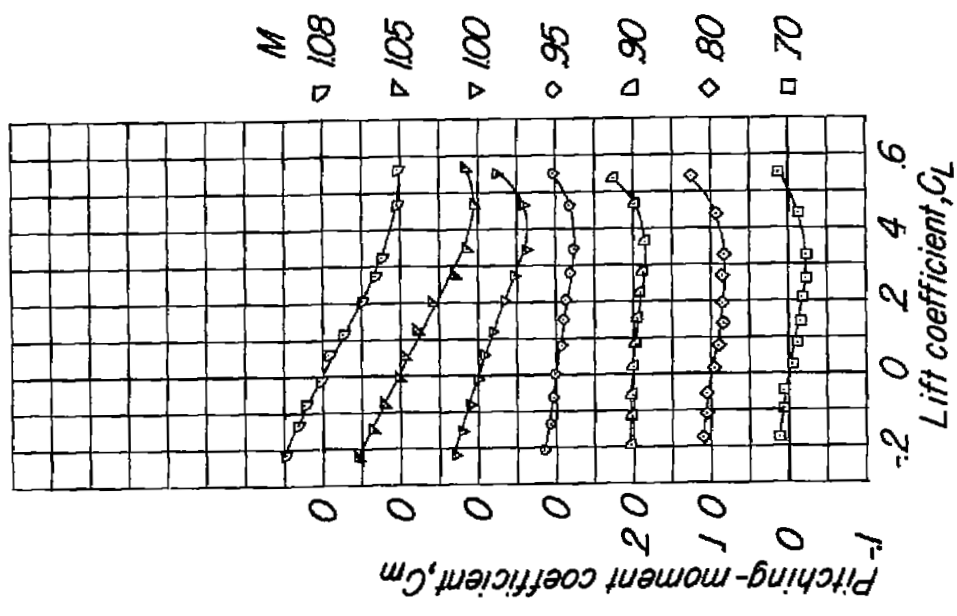

Figure 6.- Concluded.

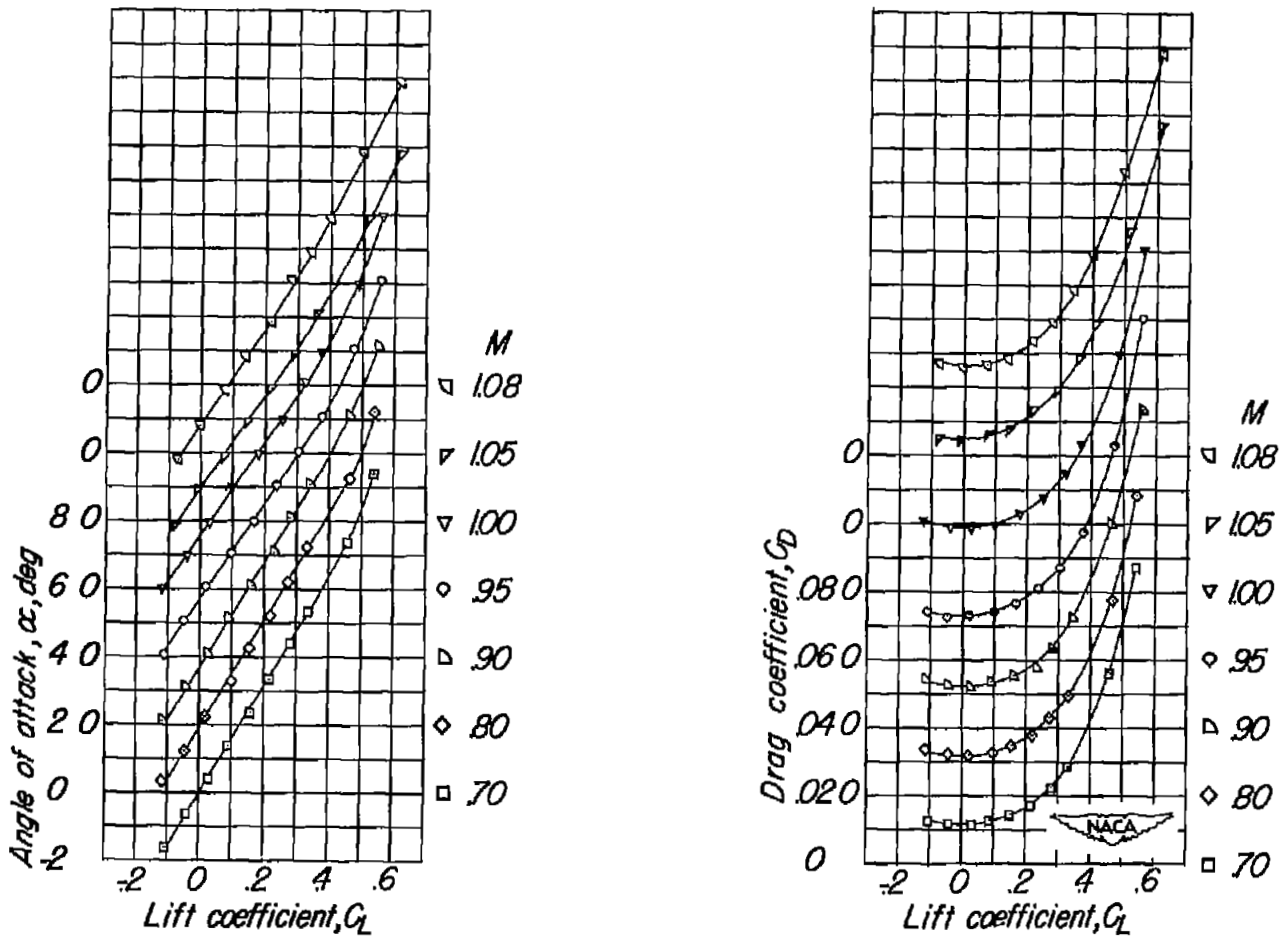

(a) Rearward chordwise position of nacelle.

Figure 7.- Aerodynamic characteristics of semispan wing with ogive-cylinder nacelle at $\frac{y}{b/2} = 0.46$.

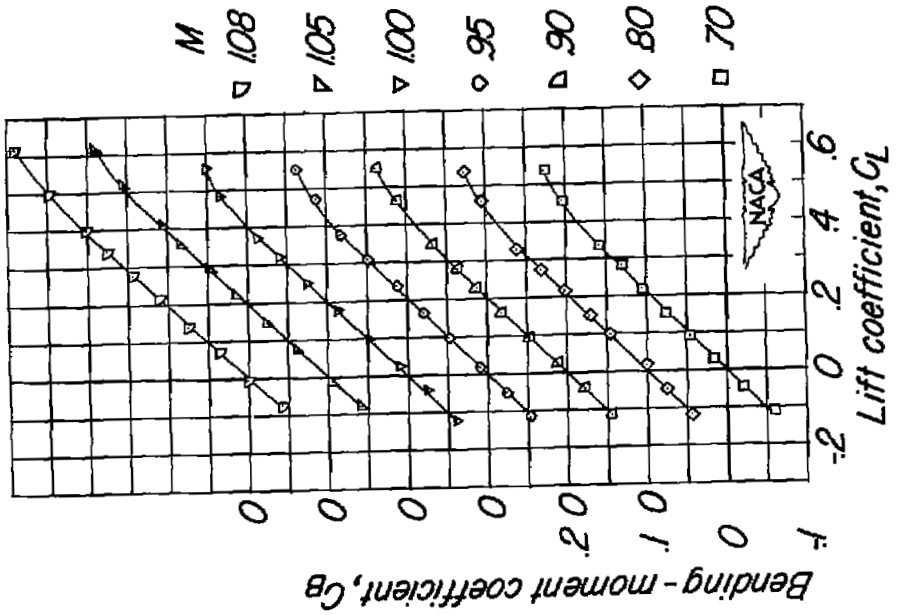

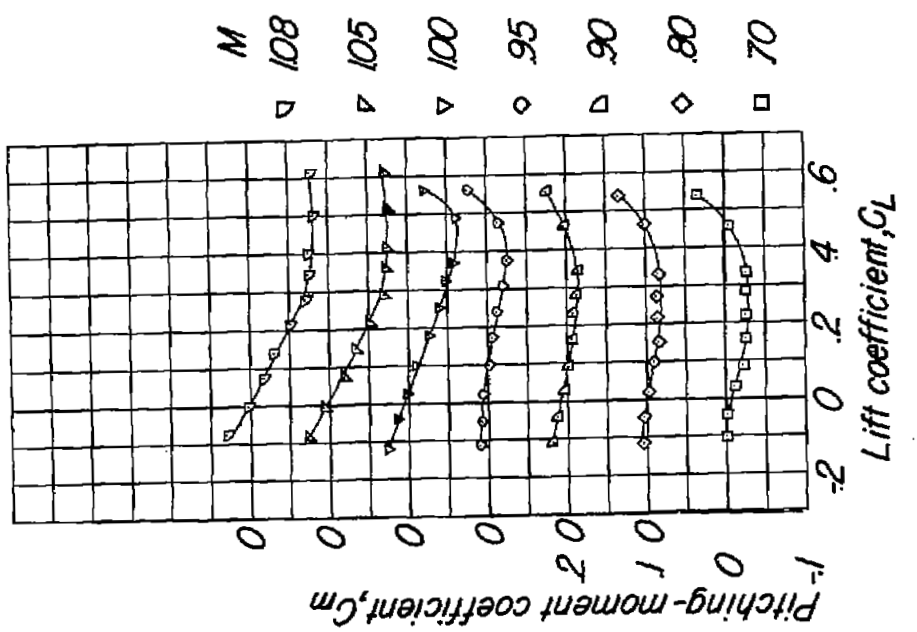

(a) Concluded.

Figure 7.- Continued.

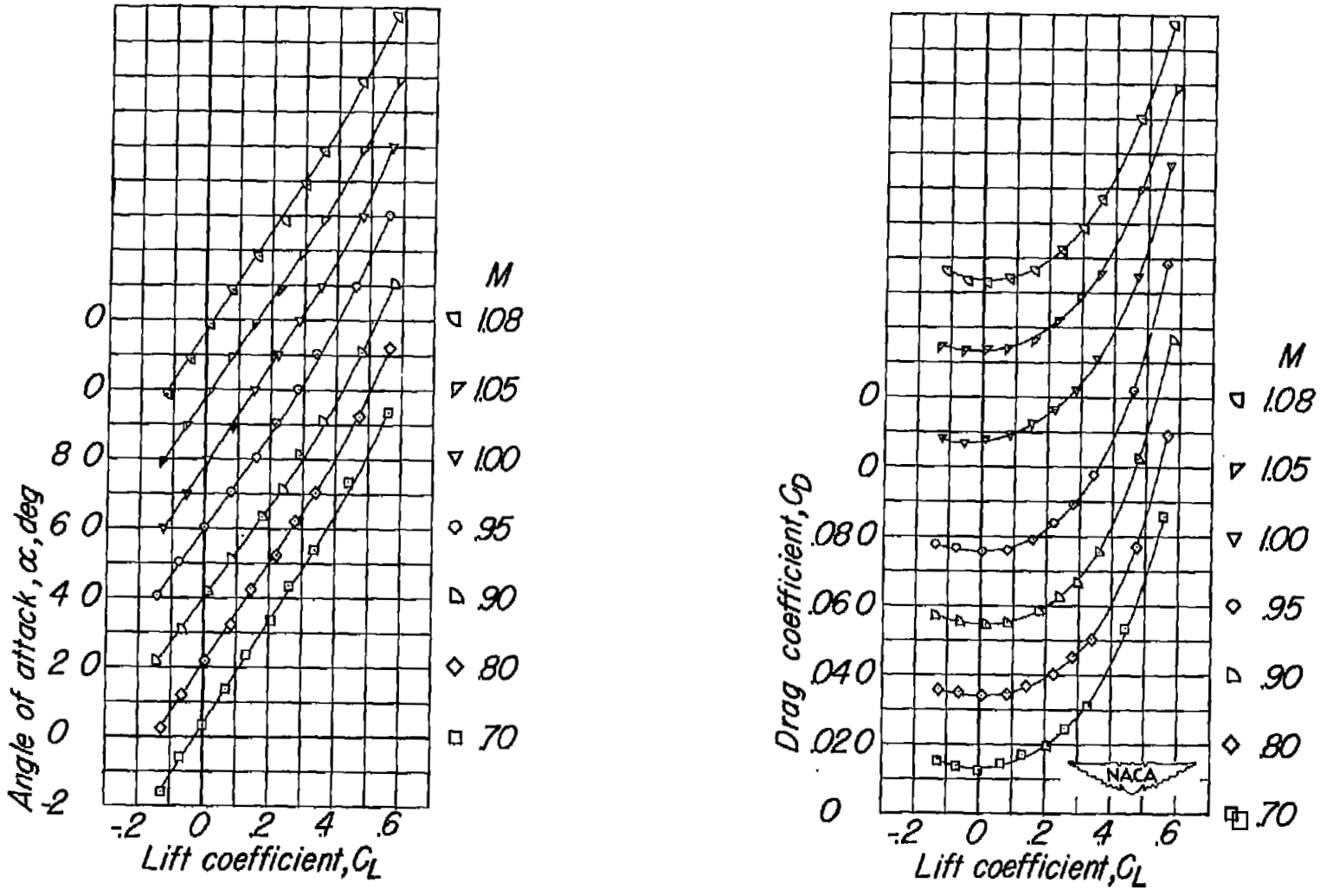

(b) Intermediate chordwise position of nacelle.

Figure 7.- Continued.

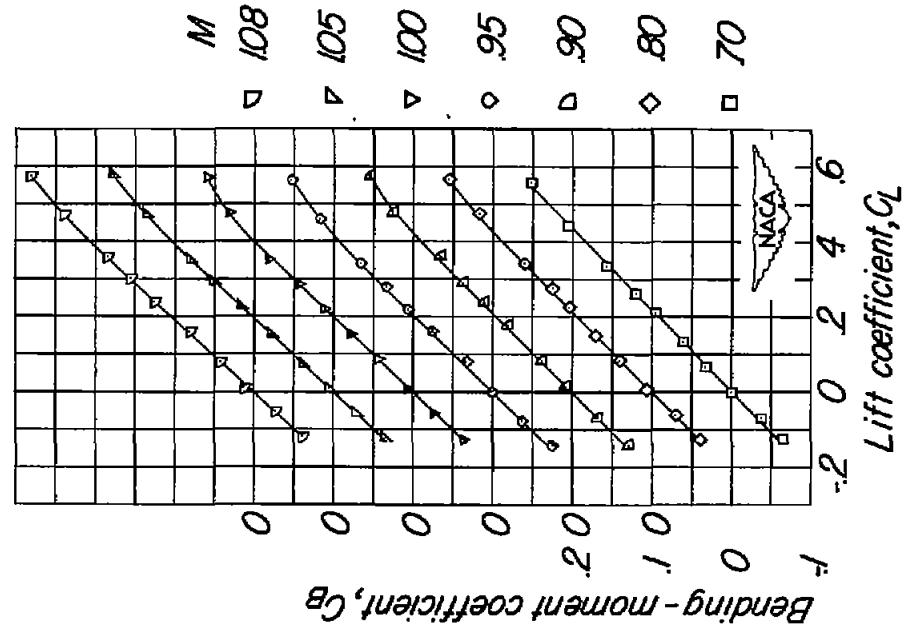

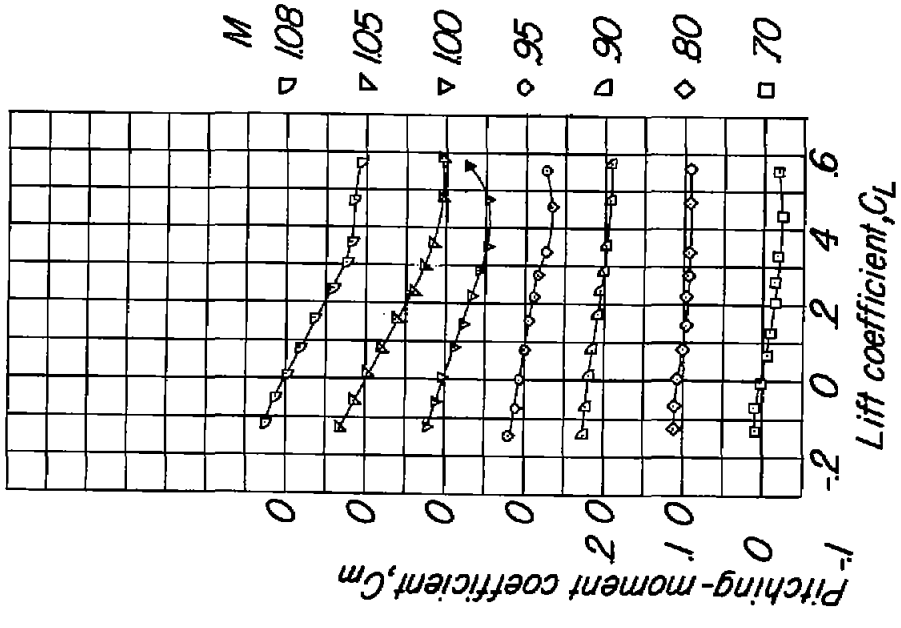

(b) Concluded.

Figure 7.- Continued.

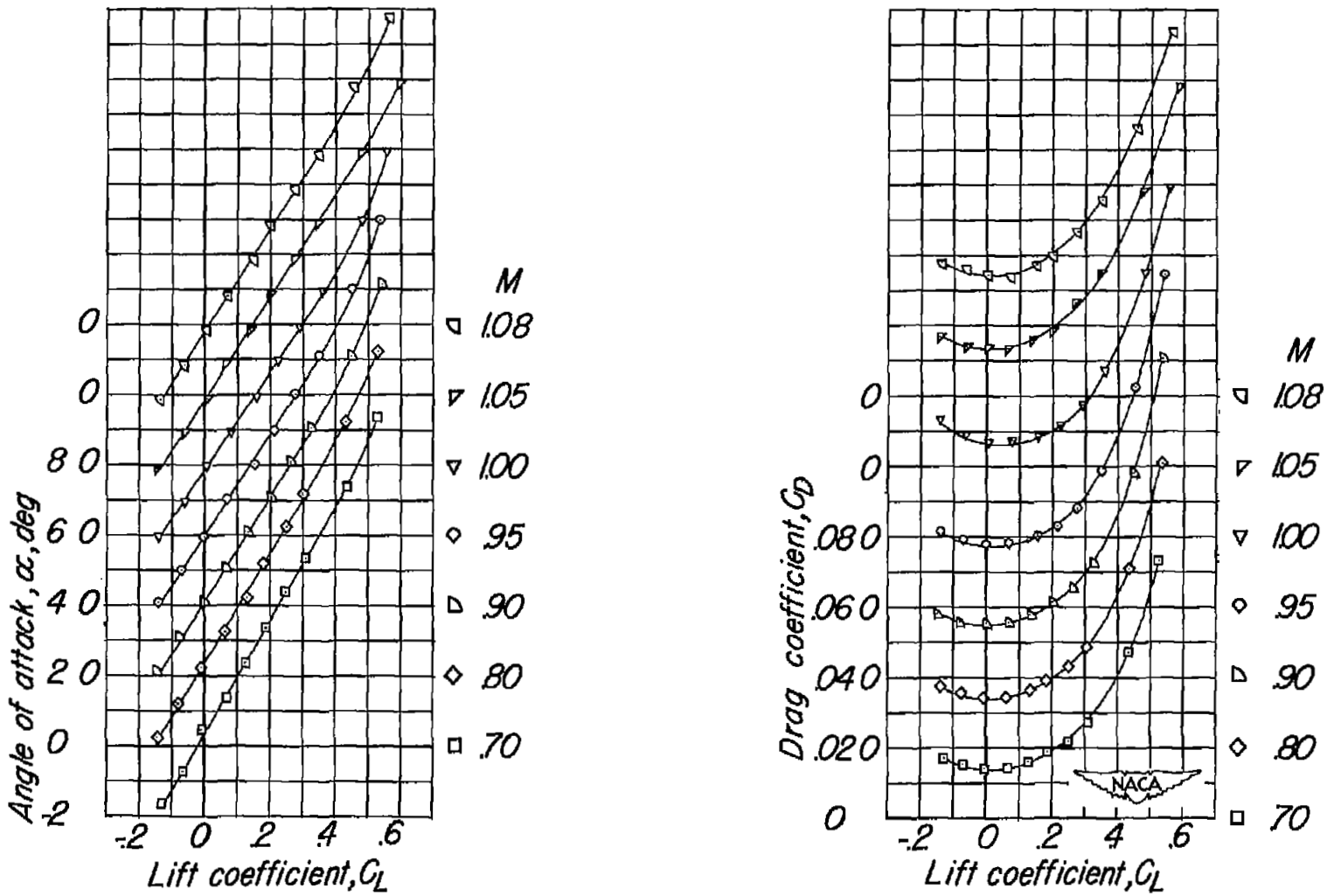

(c) Forward chordwise position of nacelle.

Figure 7.- Continued.

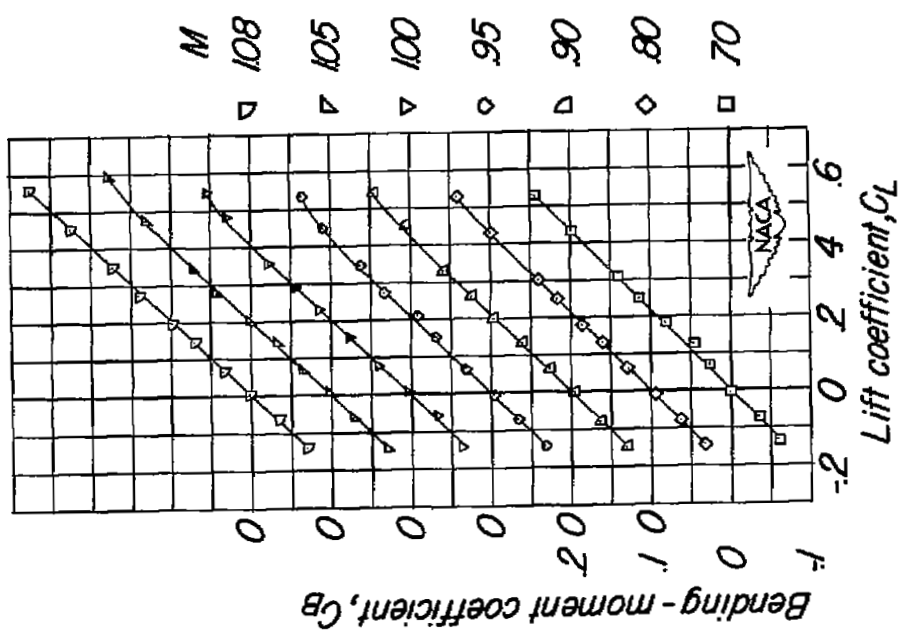

(c) Concluded.

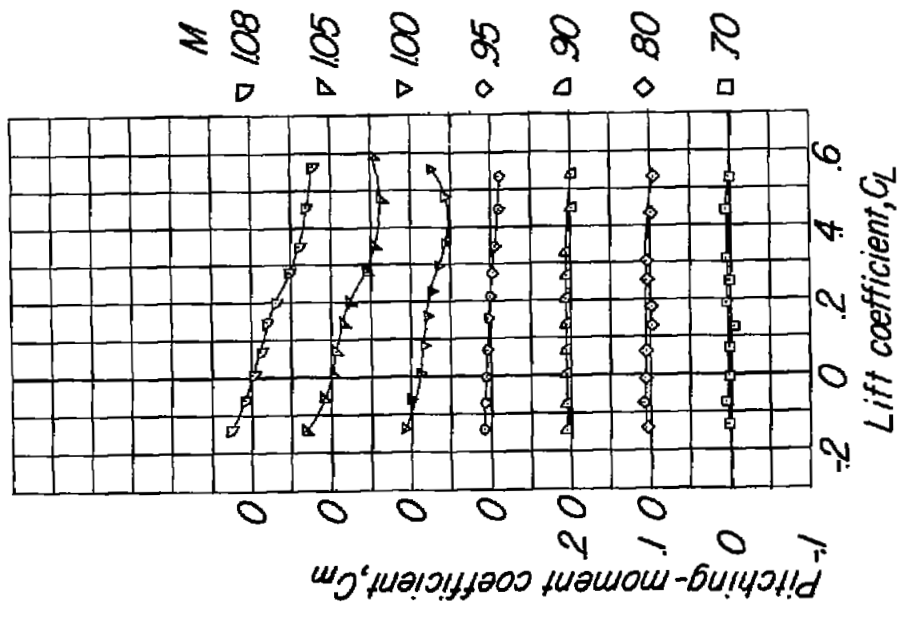

Figure 7.- Concluded.

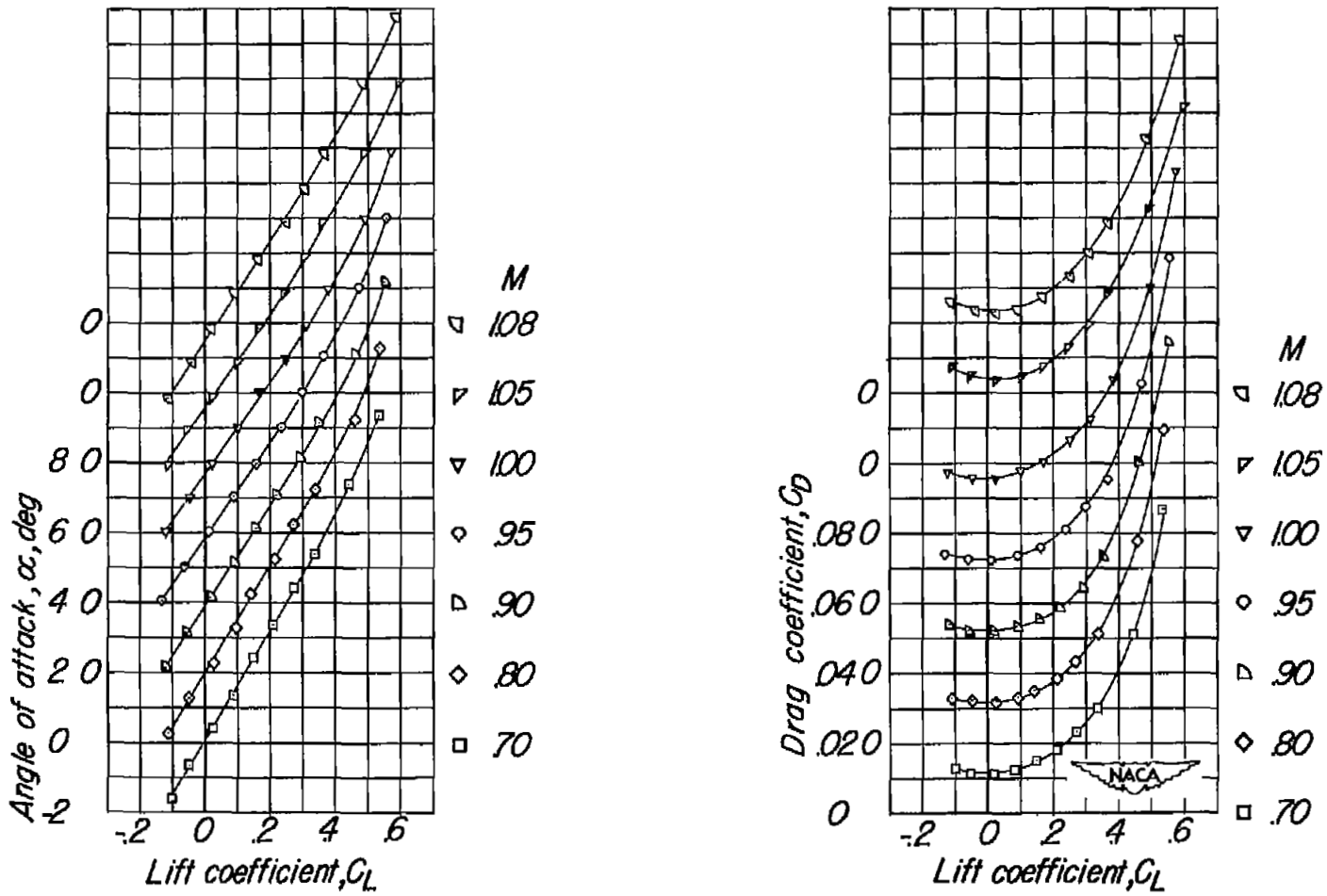

(a) Rearward chordwise position of nacelle.

Figure 8.- Aerodynamic characteristics of semispan wing with the 65A-series nacelle at $\frac{y}{b/2} = 0.46$.

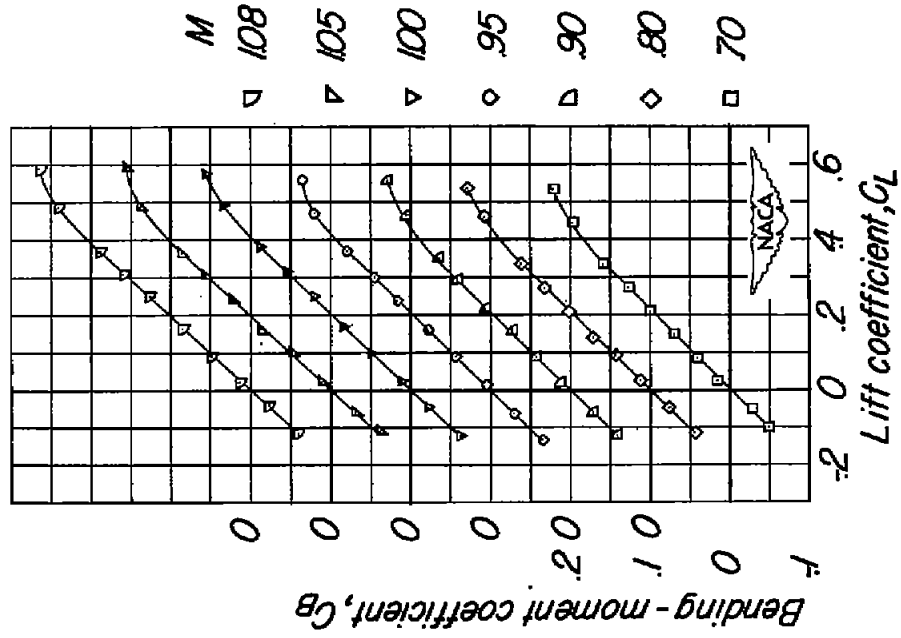

(a) Concluded.

Figure 8.- Continued.

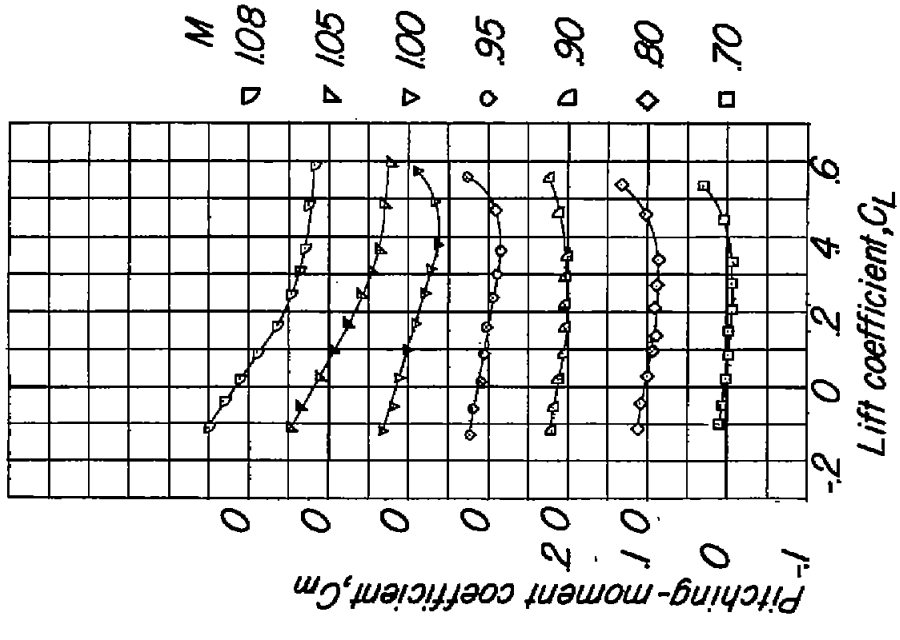

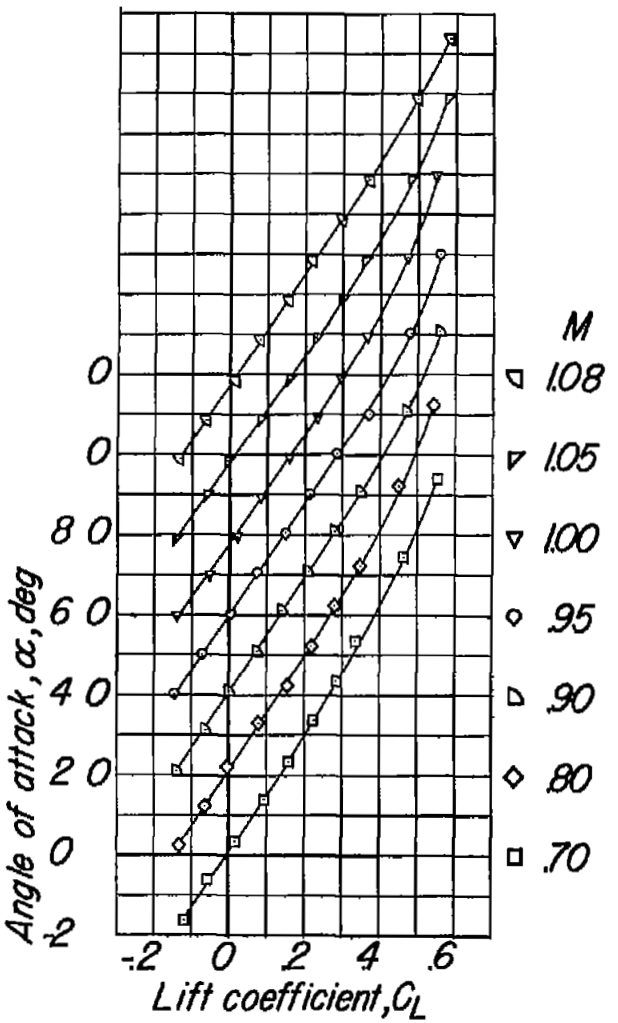

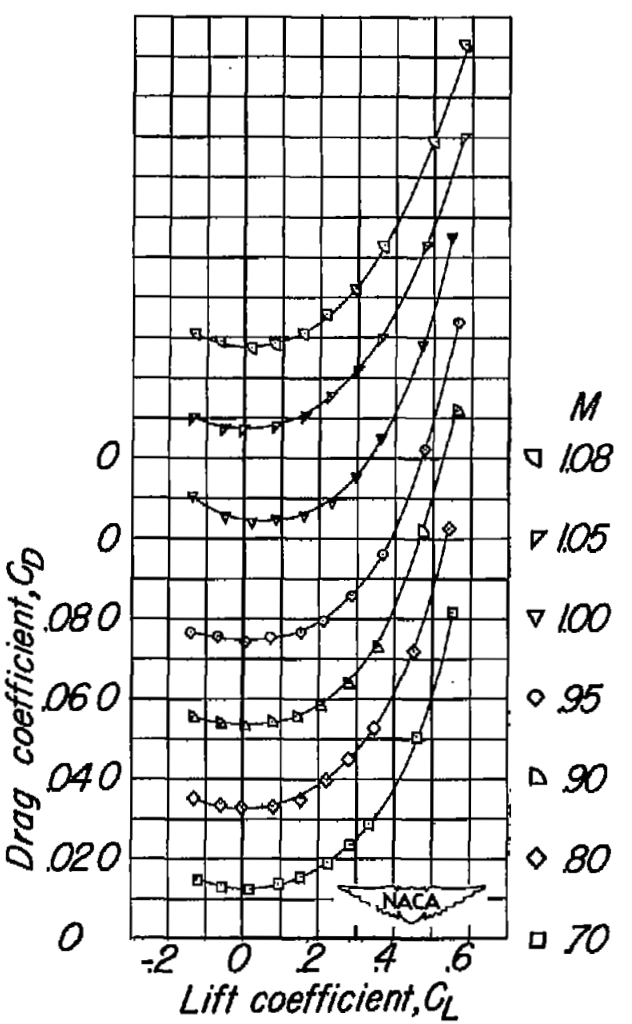

(b) Intermediate chordwise position of nacelle.

Figure 8.- Continued.

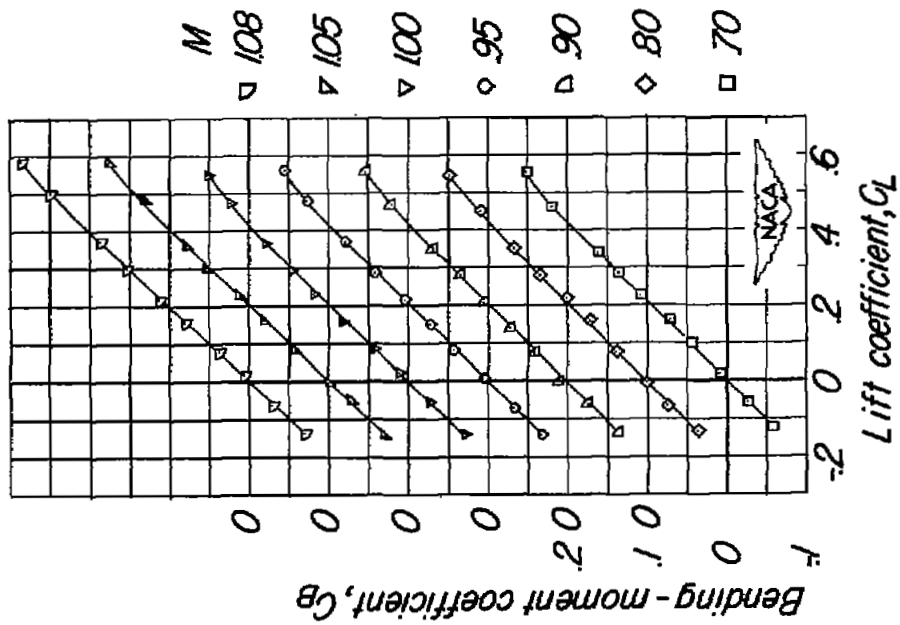

(b) Concluded.

Figure 8.- Continued.

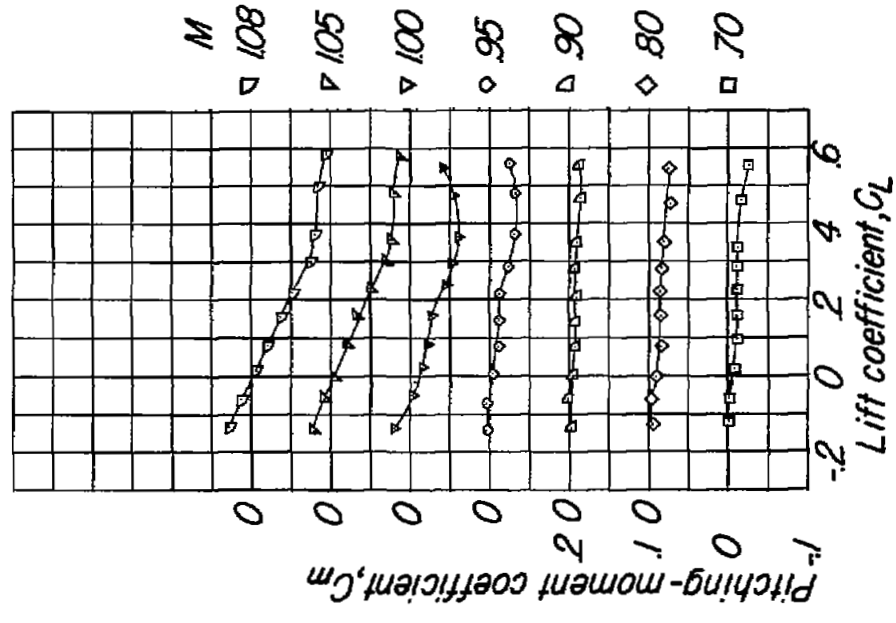

[redacted]

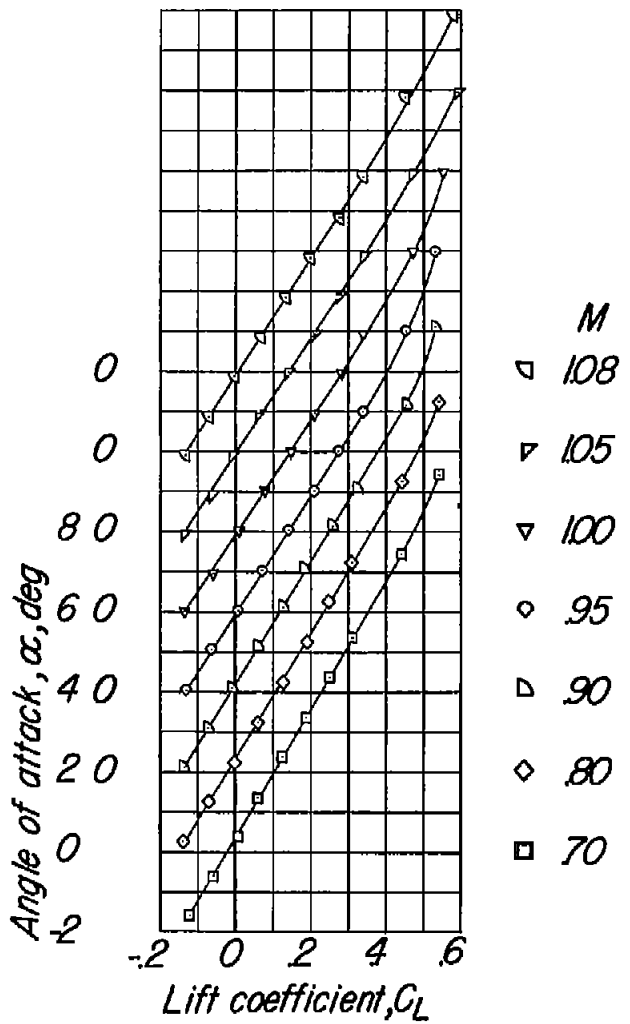

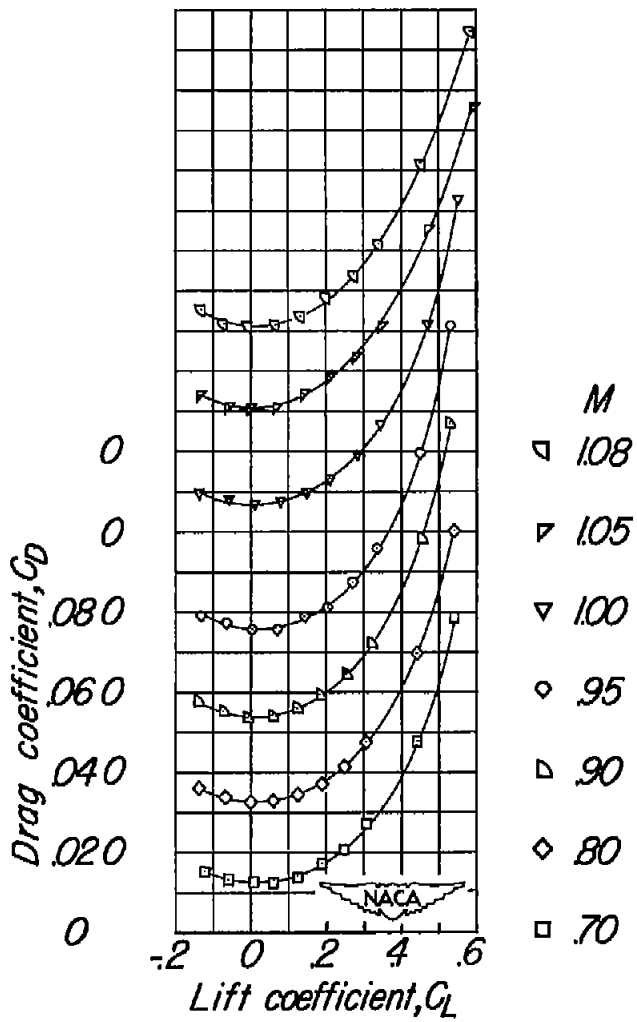

(c) Forward chordwise position of nacelle.

Figure 8.- Continued.

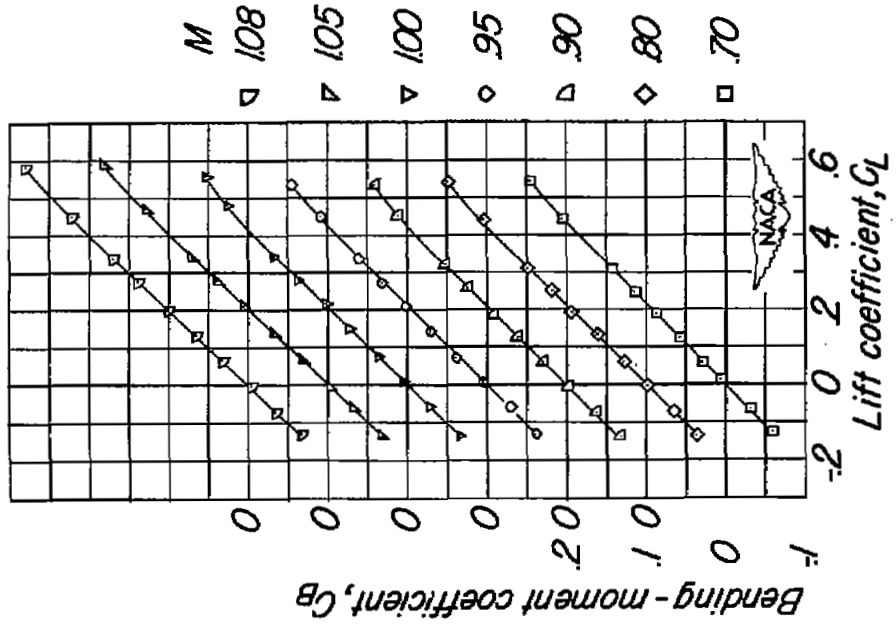

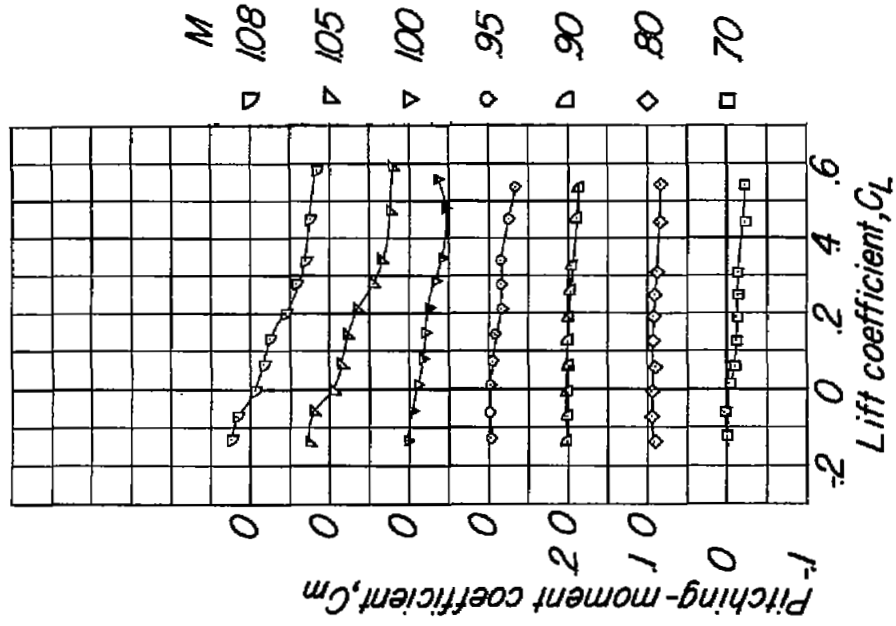

(c) Concluded.

Figure 8.- Concluded.

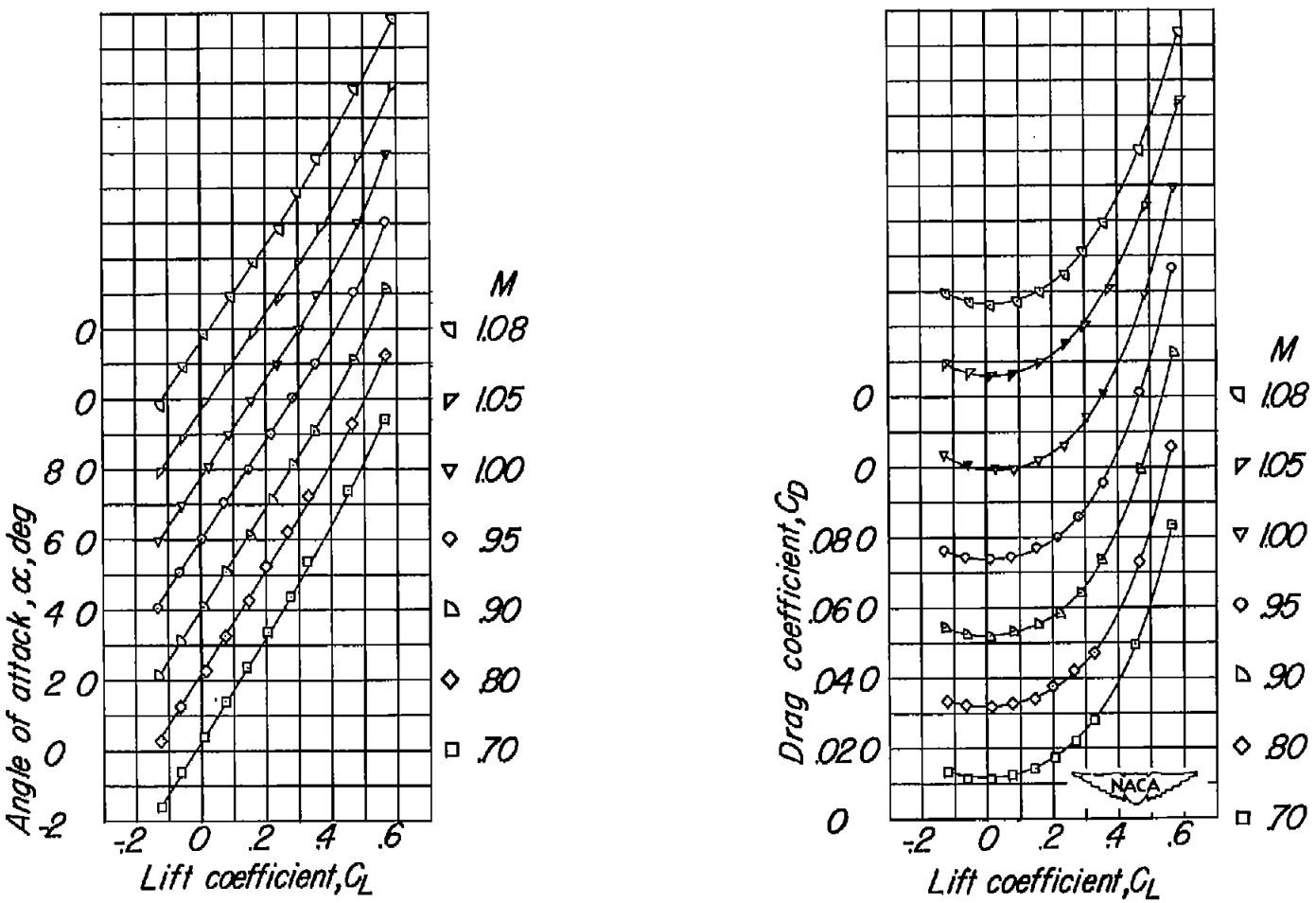

(a) Rearward chordwise position of nacelle.

Figure 9.- Aerodynamic characteristics of the semispan wing with the 0-series nacelle at $\frac{y}{b/2} = 0.46$.

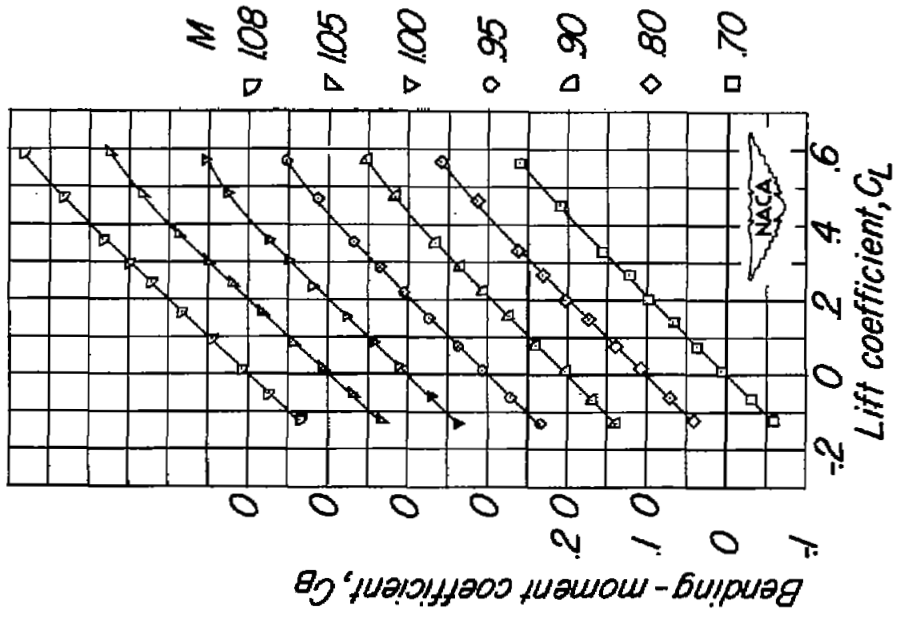

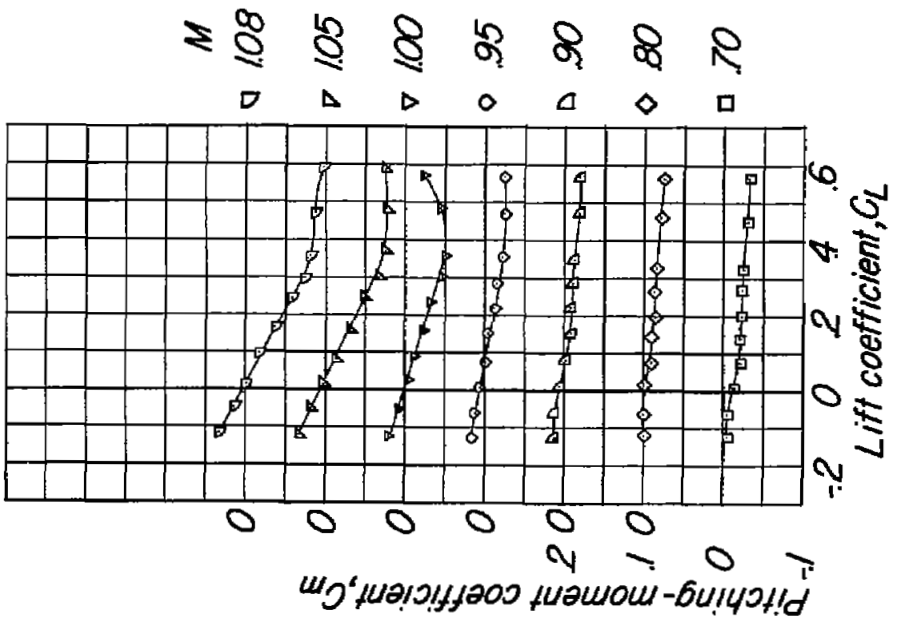

(a) Concluded.

Figure 9.- Continued.

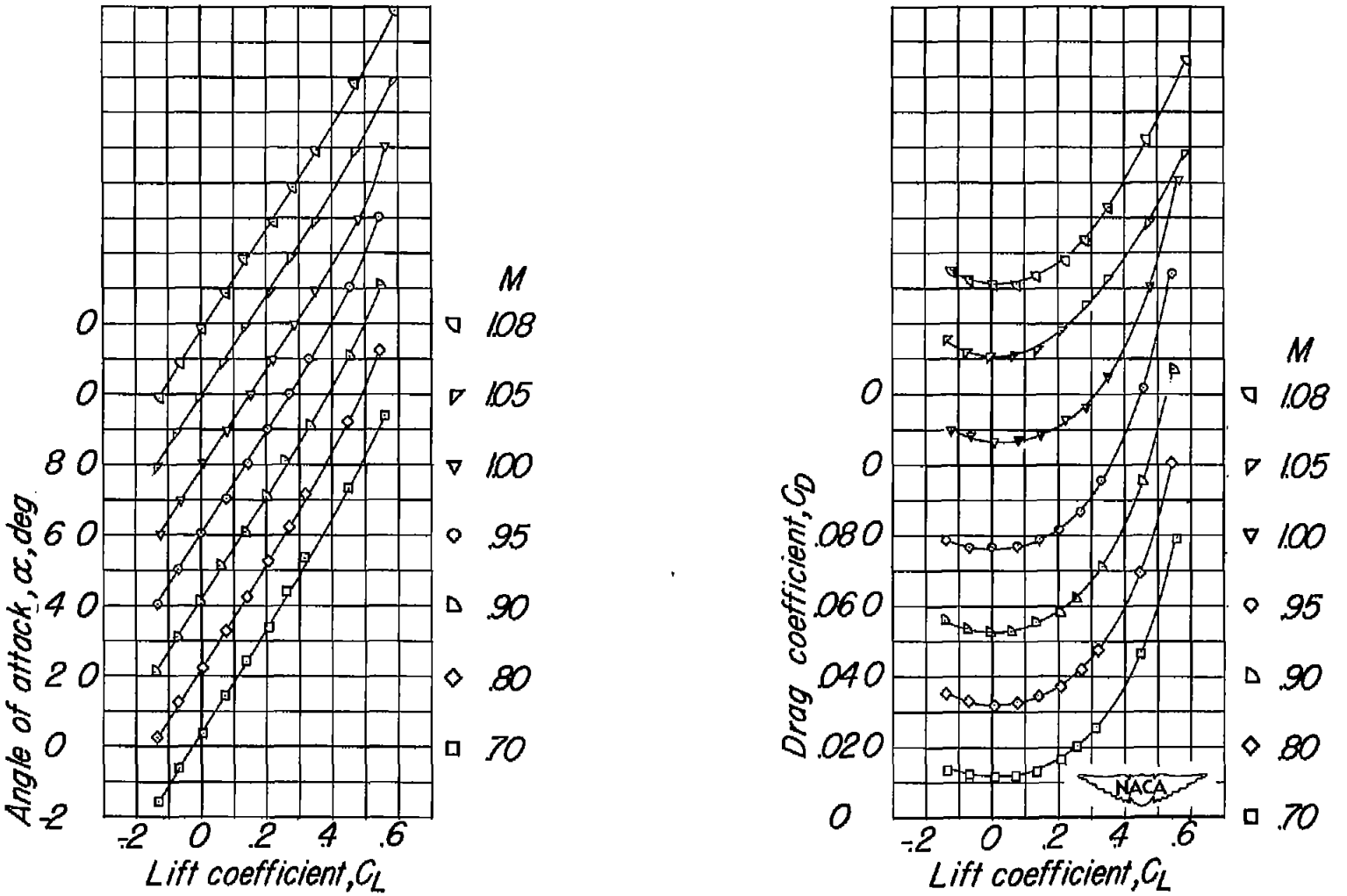

(b) Intermediate chordwise position of nacelle.

Figure 9.- Continued.

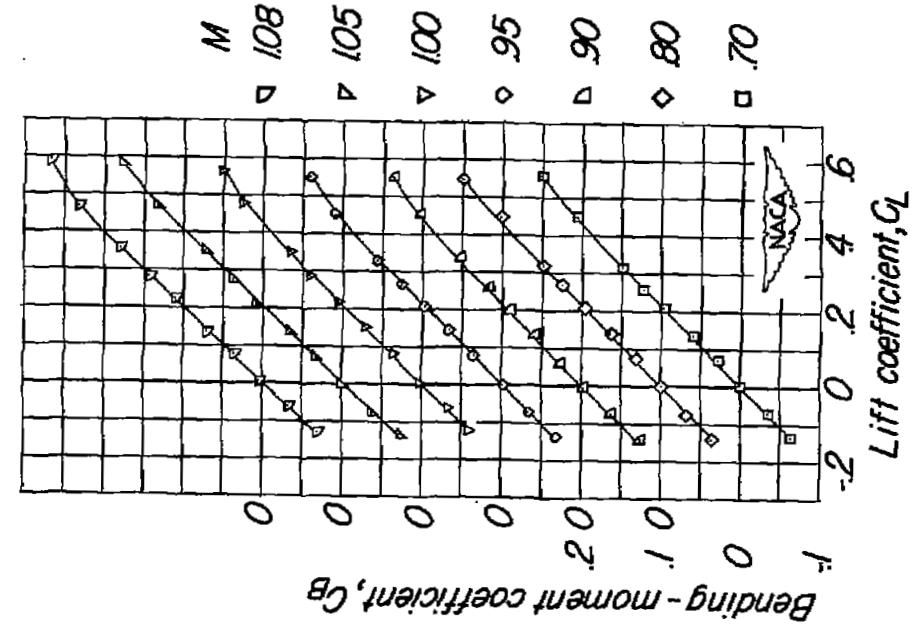

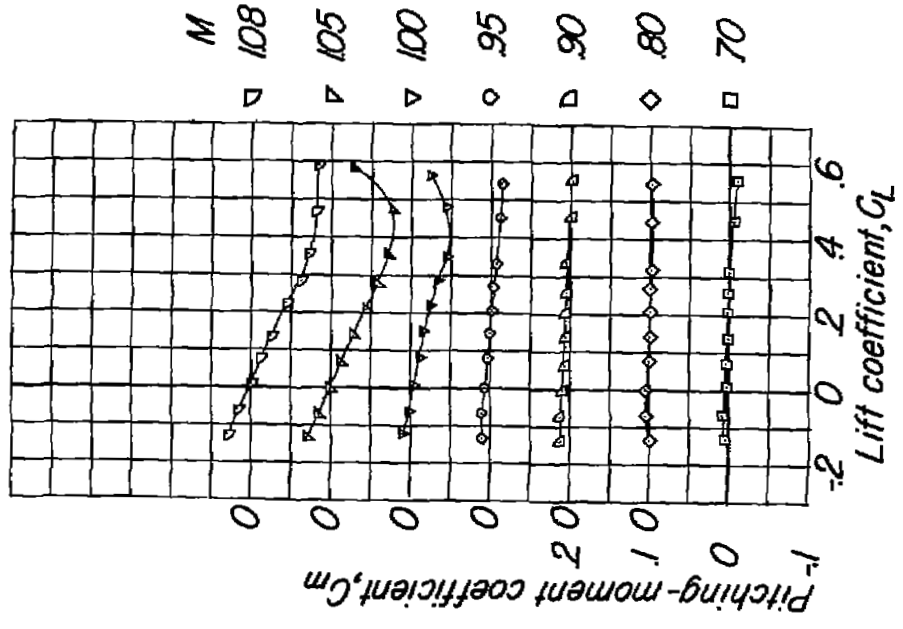

(b) Concluded.

Figure 9.- Continued.

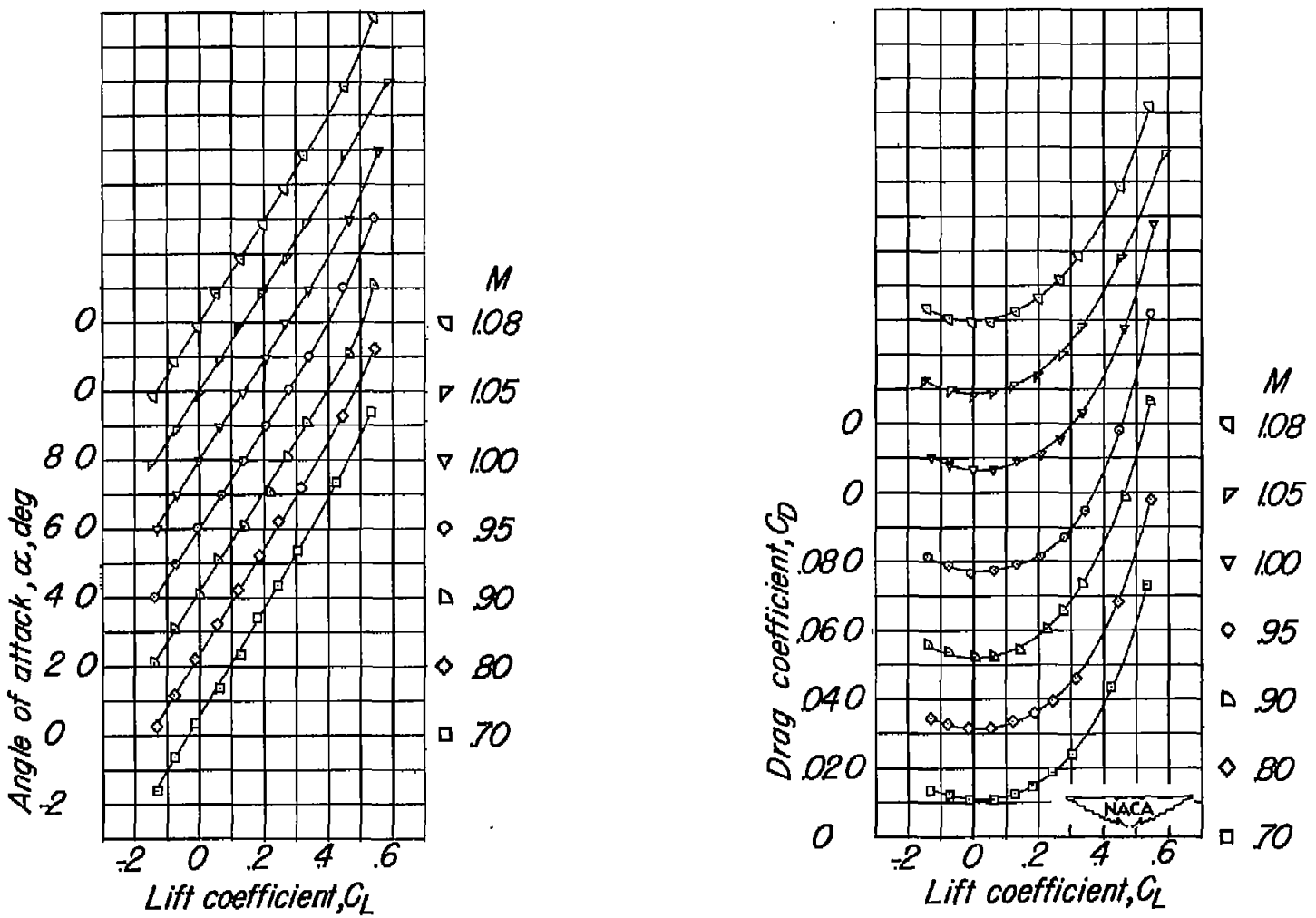

(c) Forward chordwise position of nacelle.

Figure 9.- Continued.

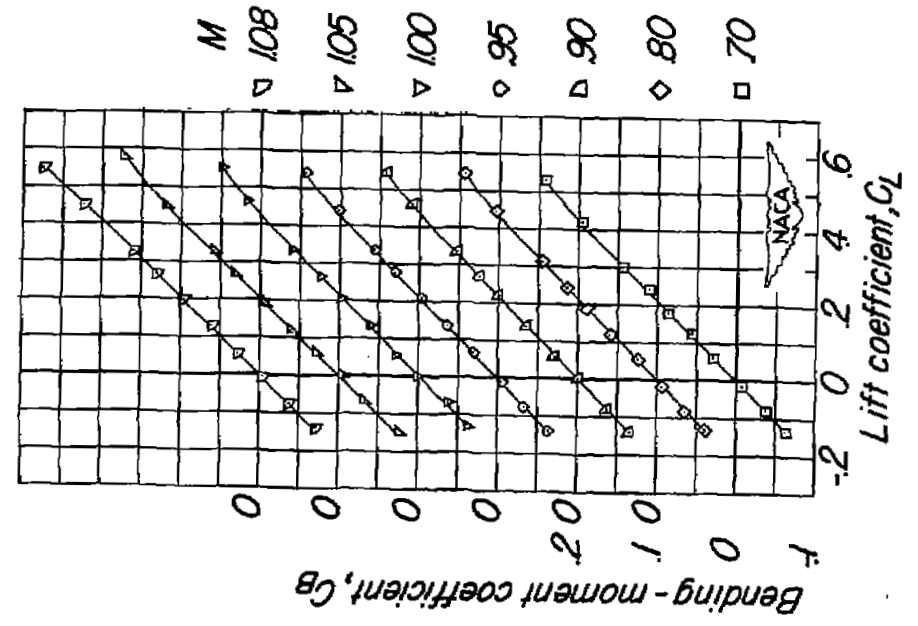

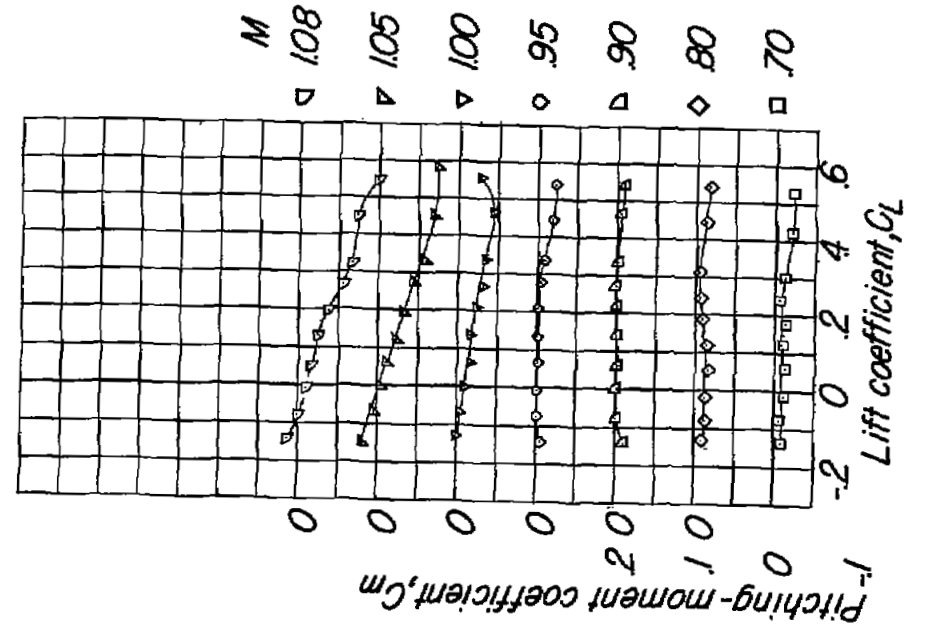

(c) Concluded.

Figure 9.- Concluded.

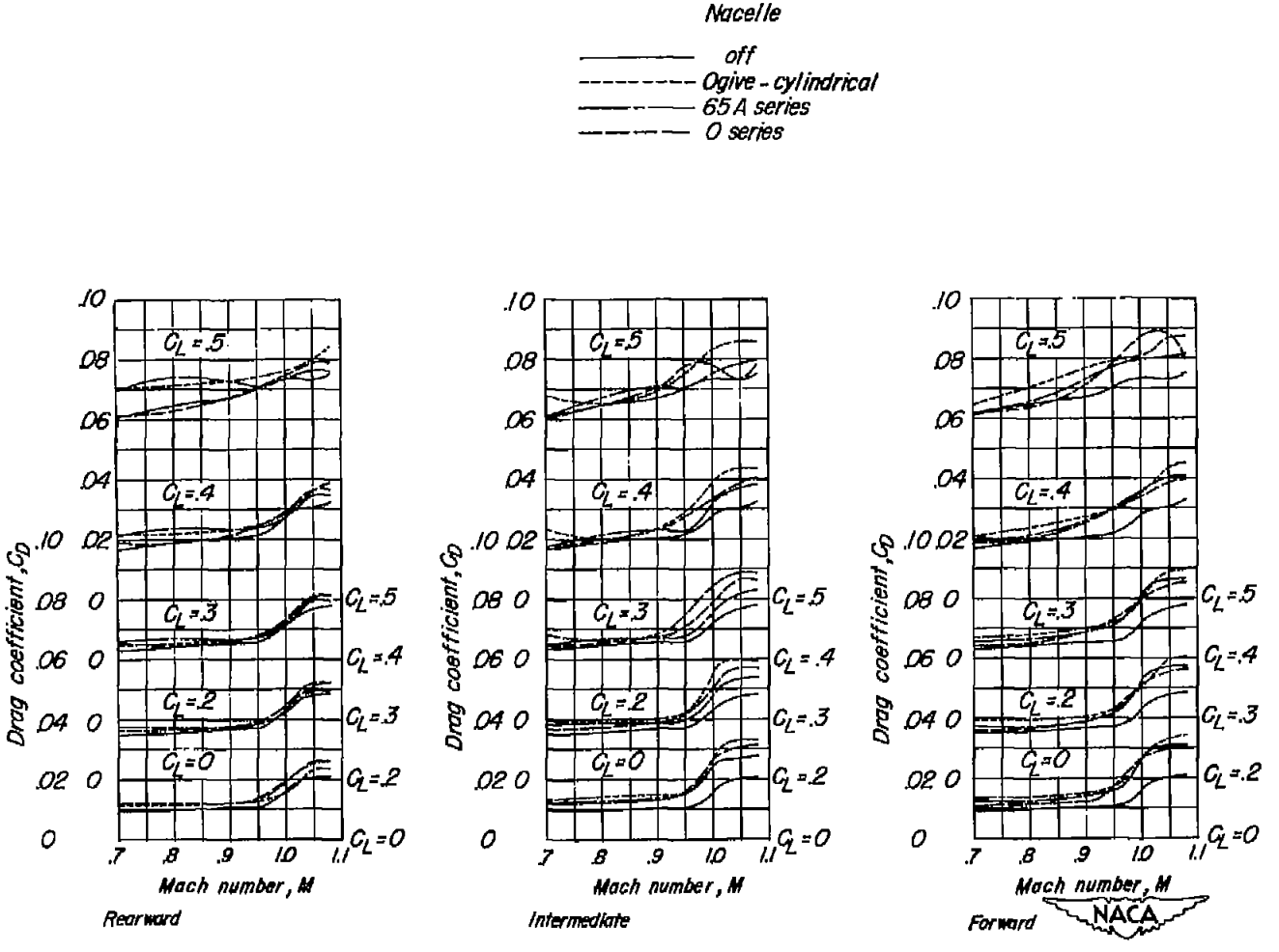

Figure 10.- Variation of drag coefficient with Mach number for semispan wing alone and with the three nacelle shapes in various chordwise locations at $\frac{y}{b/2} = 0.46$.

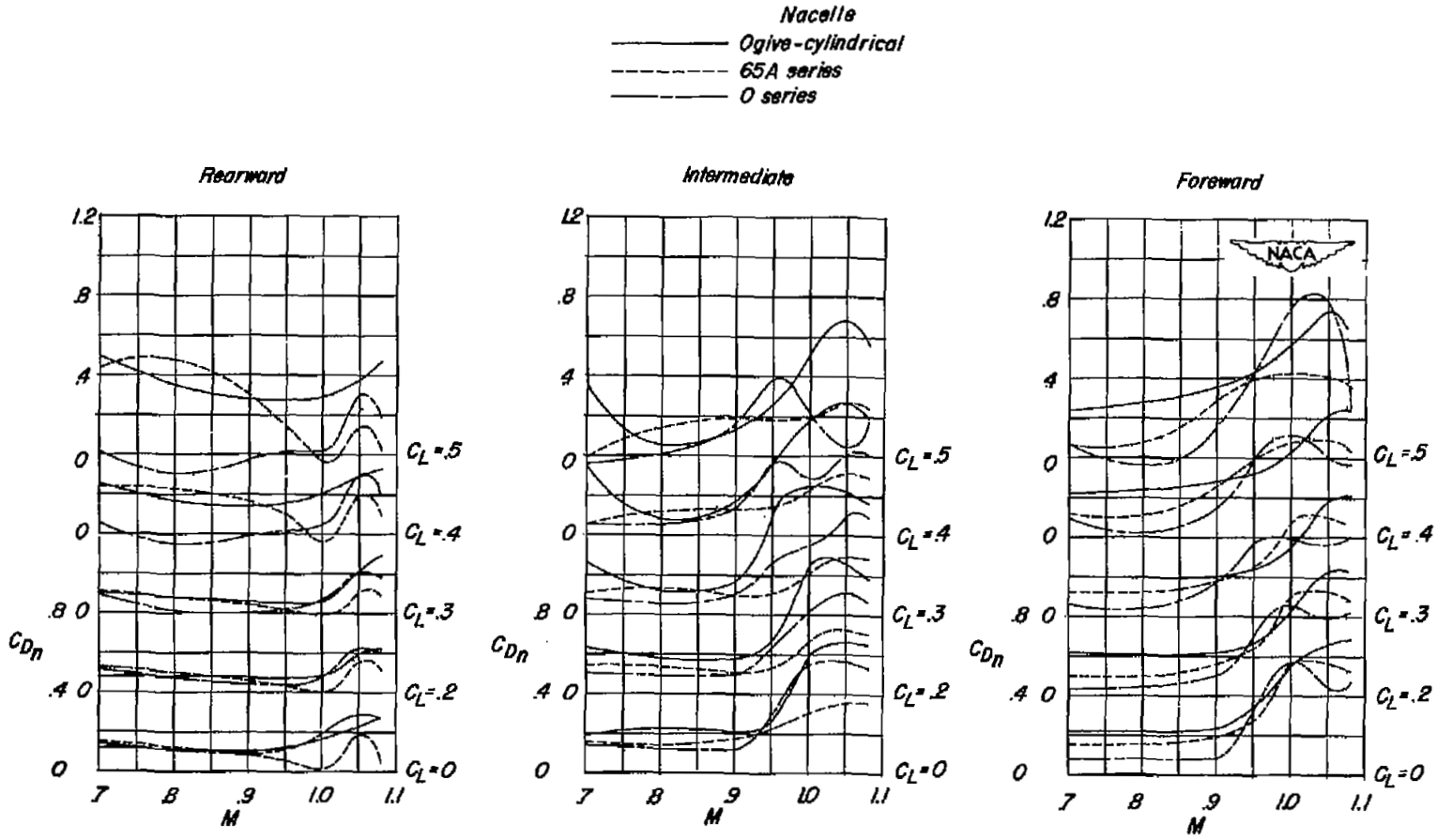

Figure 11.- Variation of nacelle-drag coefficient with Mach number for the three nacelle shapes in various chordwise positions at $\frac{y}{b/2} = 0.46$.

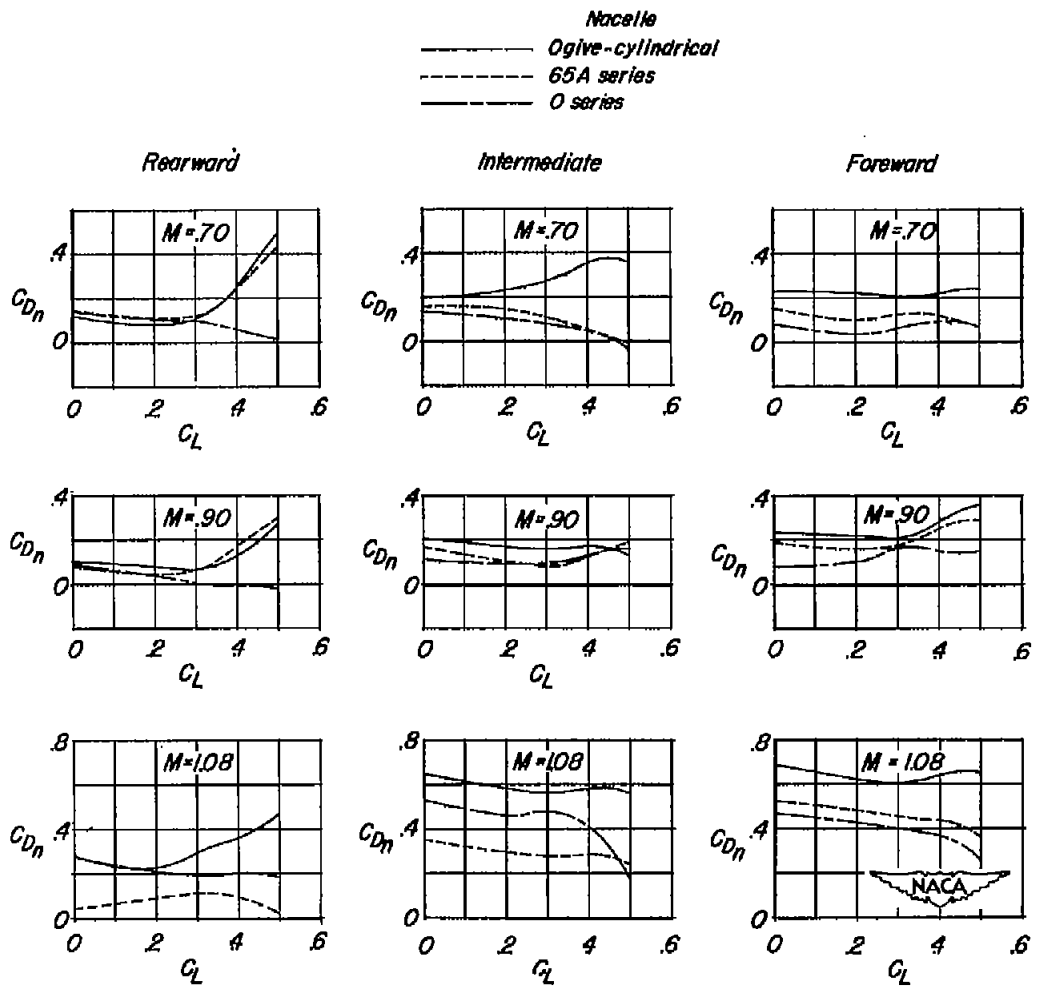

Figure 12.- Variation of nacelle-drag coefficient with model lift coefficient for three nacelle shapes in various chordwise positions at $\frac{y}{b/2} = 0.46$.

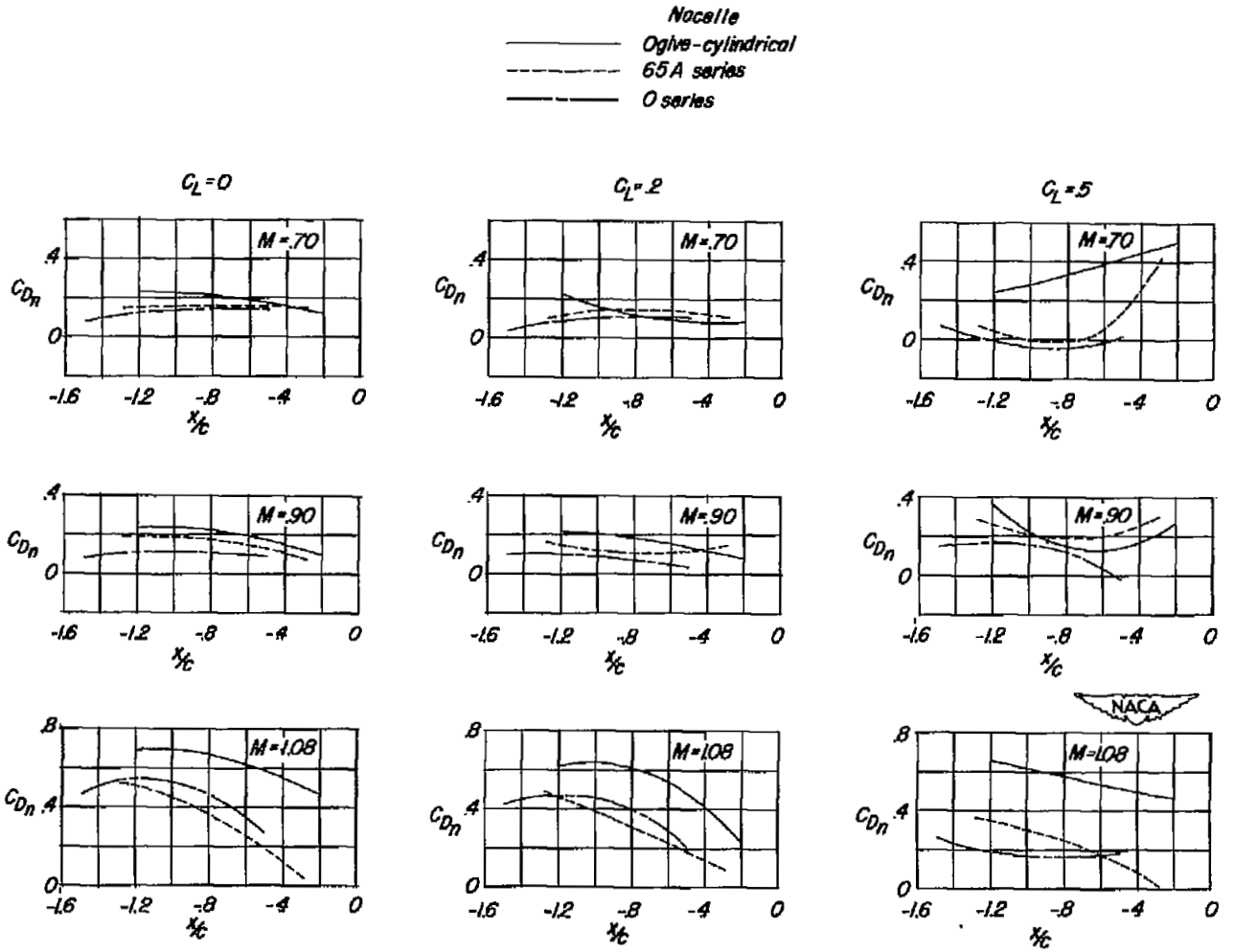

Figure 13.- Variation of nacelle-drag coefficient with nacelle chordwise position for three nacelle shapes at $\frac{y}{b/2} = 0.46$.

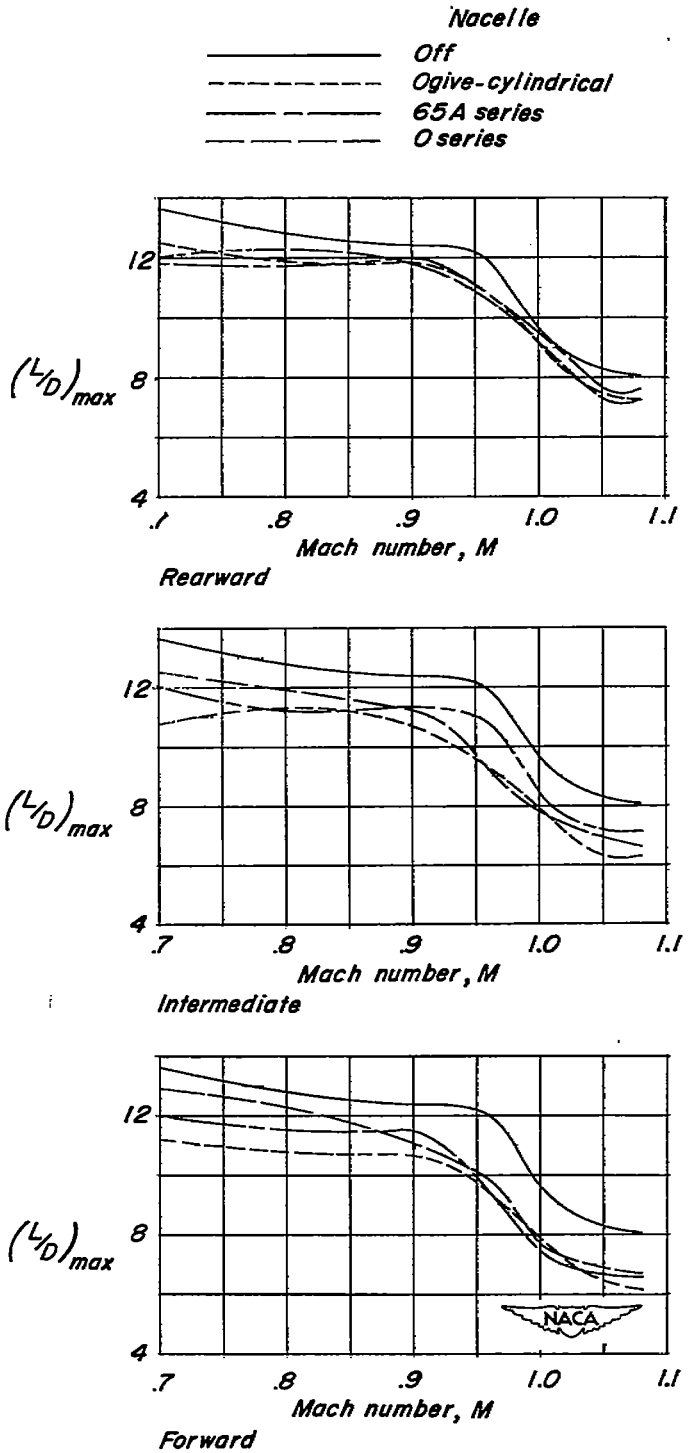

Figure 14.- Variation of the maximum lift-drag ratios with Mach number.

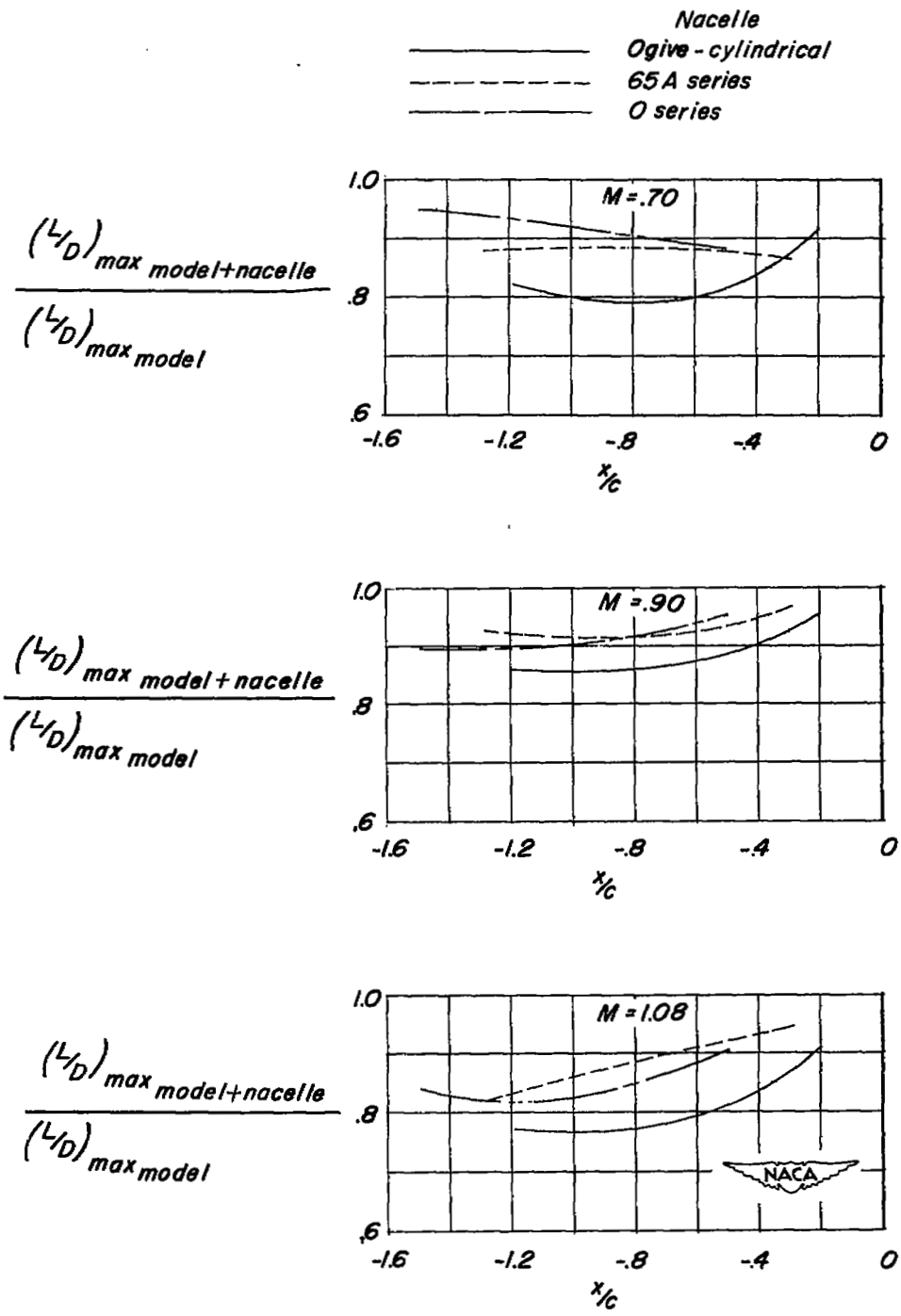

Figure 15.- Variation with chordwise position of ratios of the maximum lift-drag ratio of the model with nacelles to the maximum lift-drag ratio of the model without nacelles.

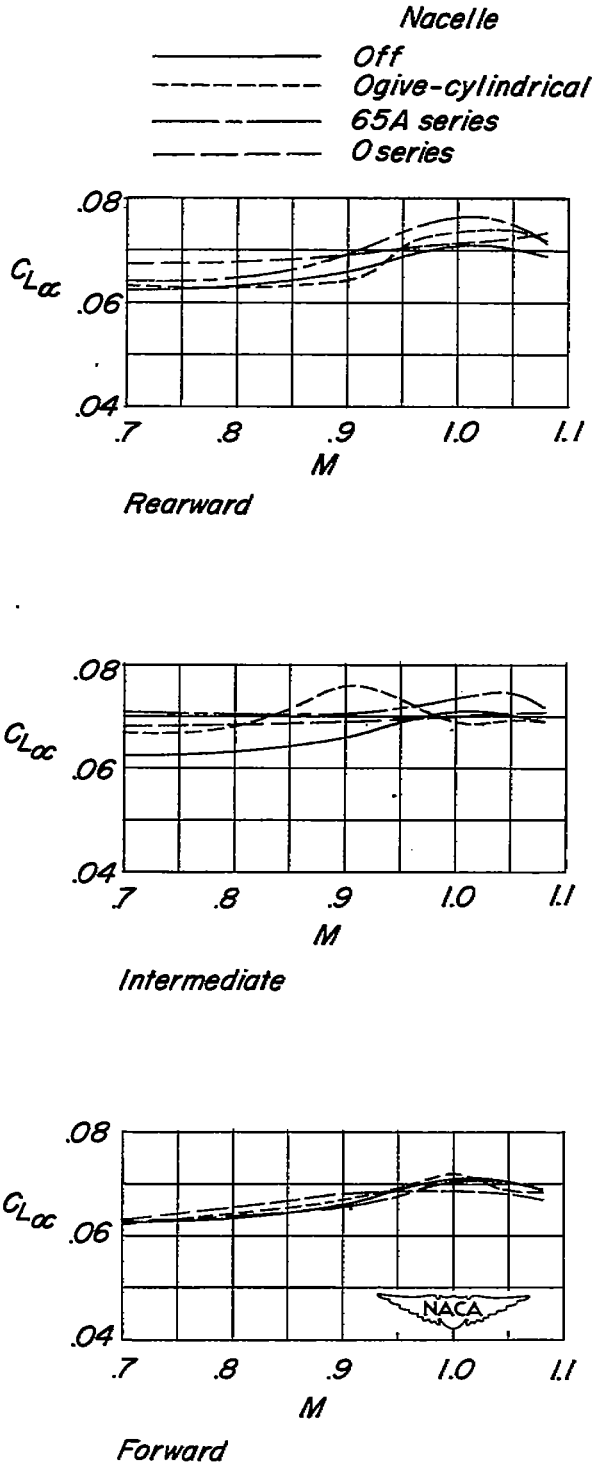

Figure 16.- Variation of the lift-curve slopes with Mach number.

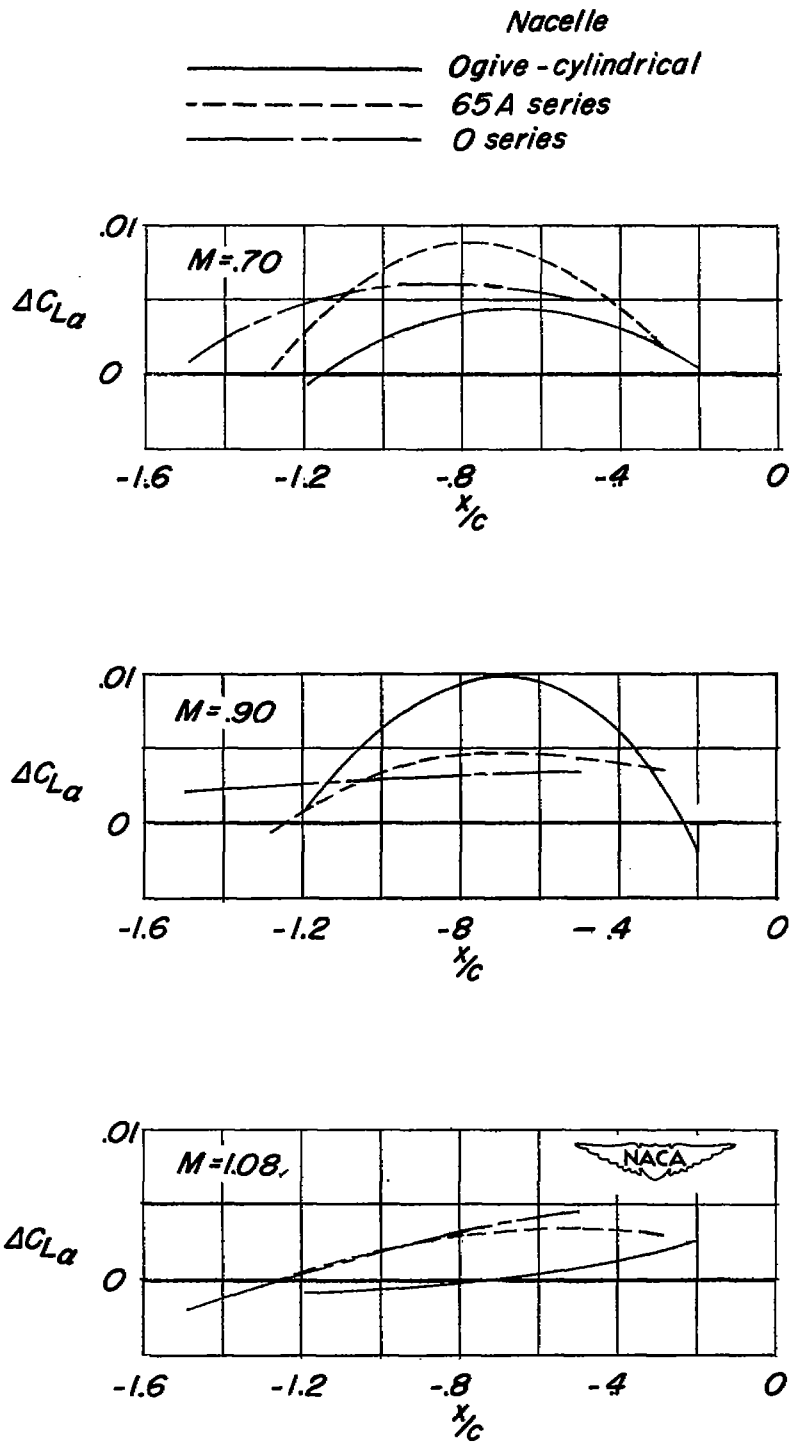

Figure 17.- Variation of the increments in lift-curve slope with nacelle chordwise position.

[redacted]

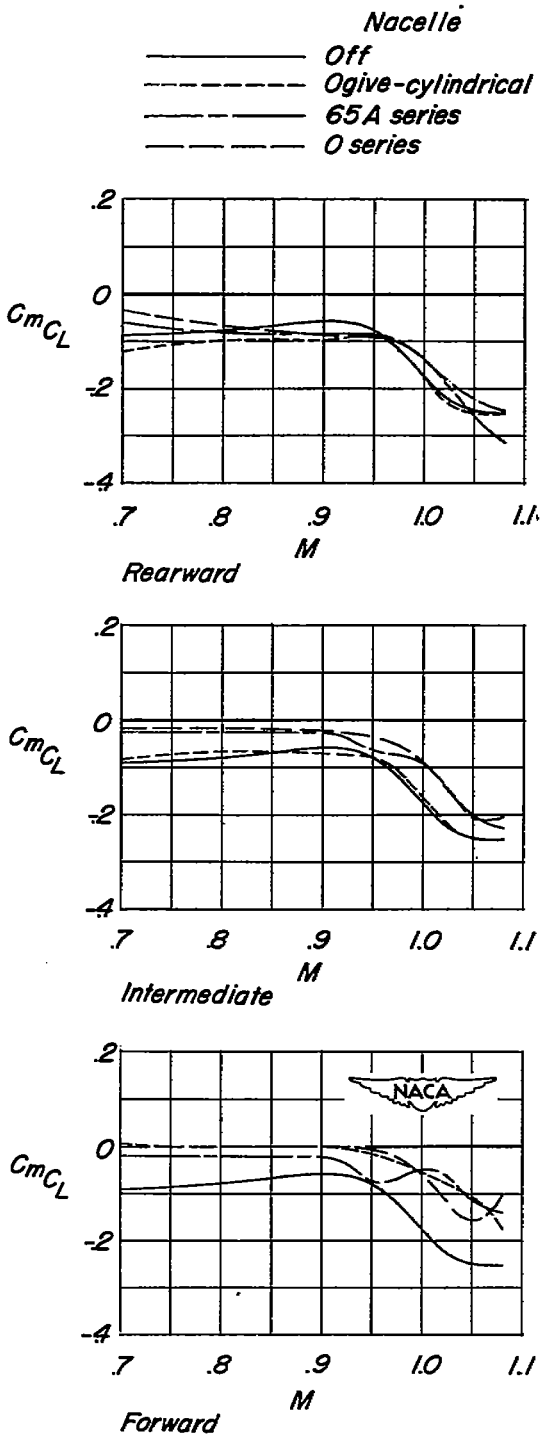

Figure 18.- Variation of the pitching-moment-curve slopes with Mach number. $C_L = 0.1$.

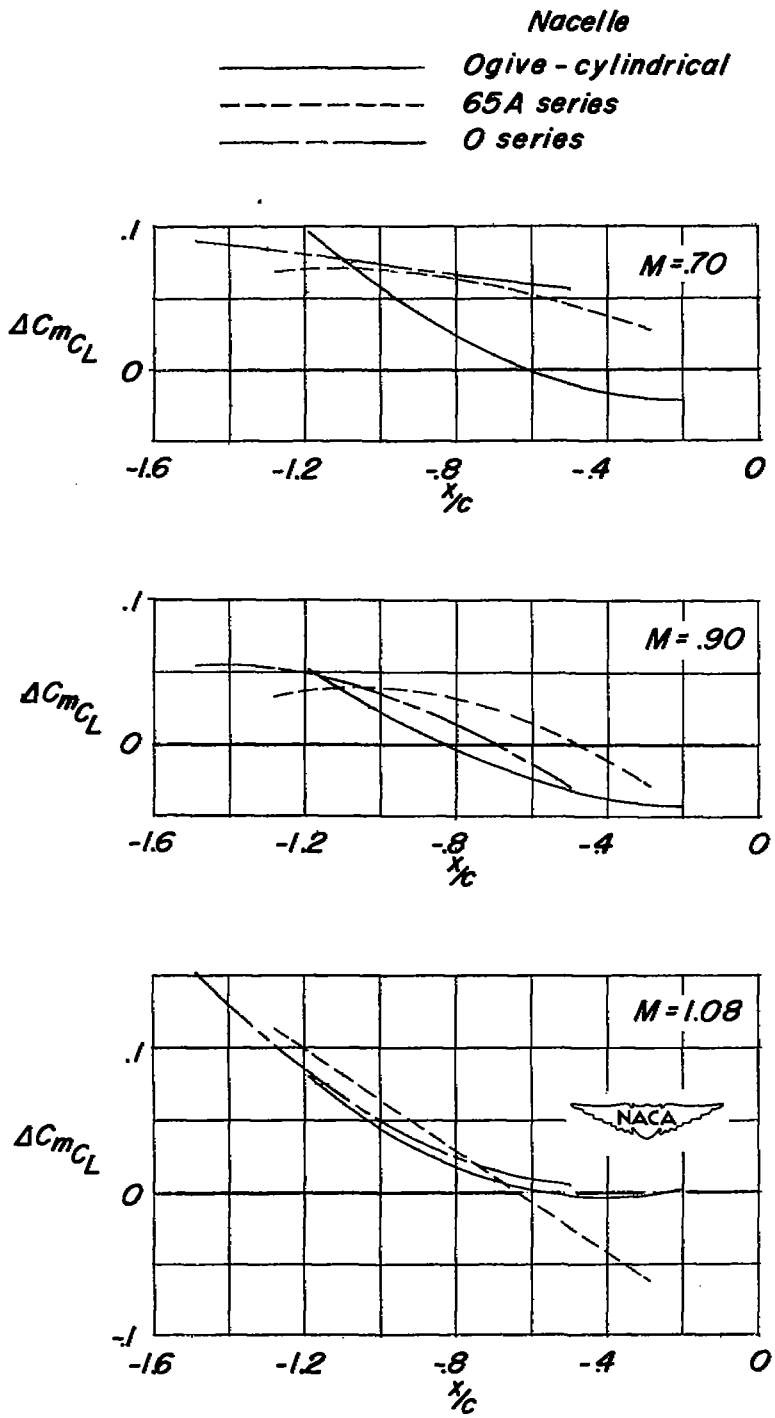

Figure 19.- Variation of the increments in pitching-moment-curve slopes with nacelle chordwise position. $C_L = 0.1$.

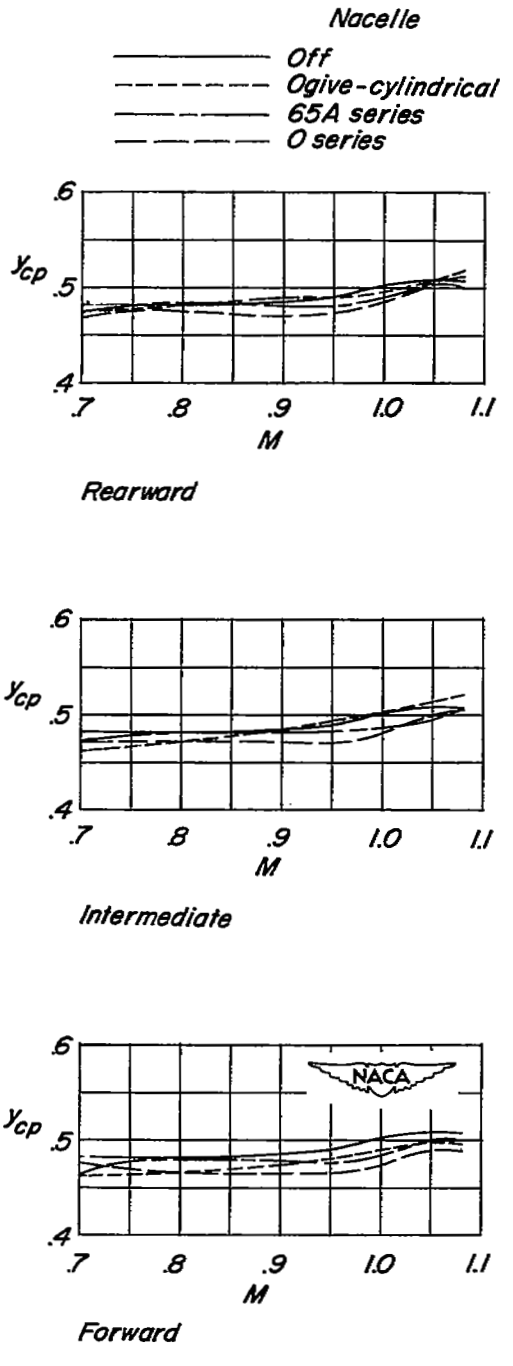

Figure 20.- Variation of the lateral-center-of-pressure locations with Mach number.

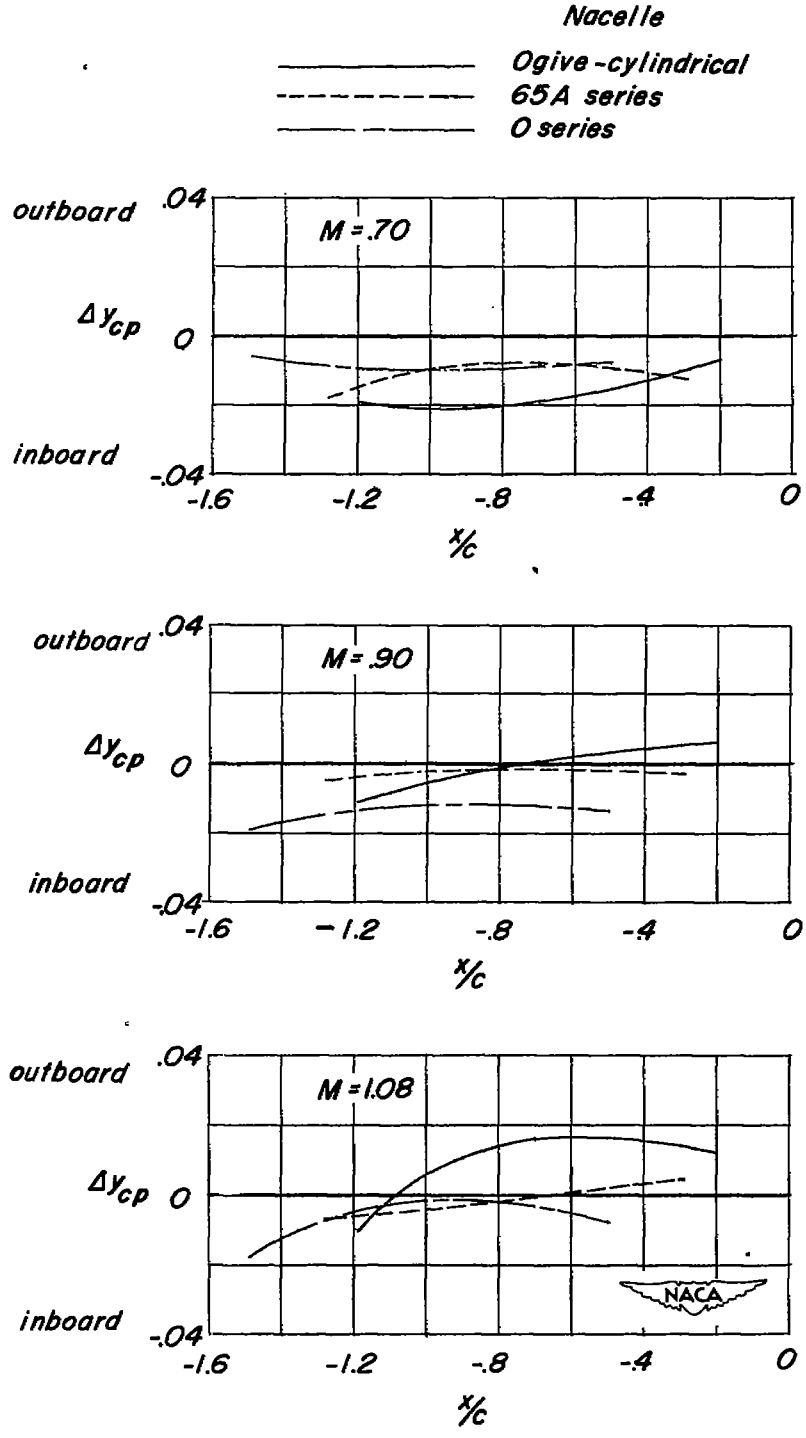

Figure 21.- Variation of the increments of lateral-center-of-pressure locations with nacelle chordwise position.